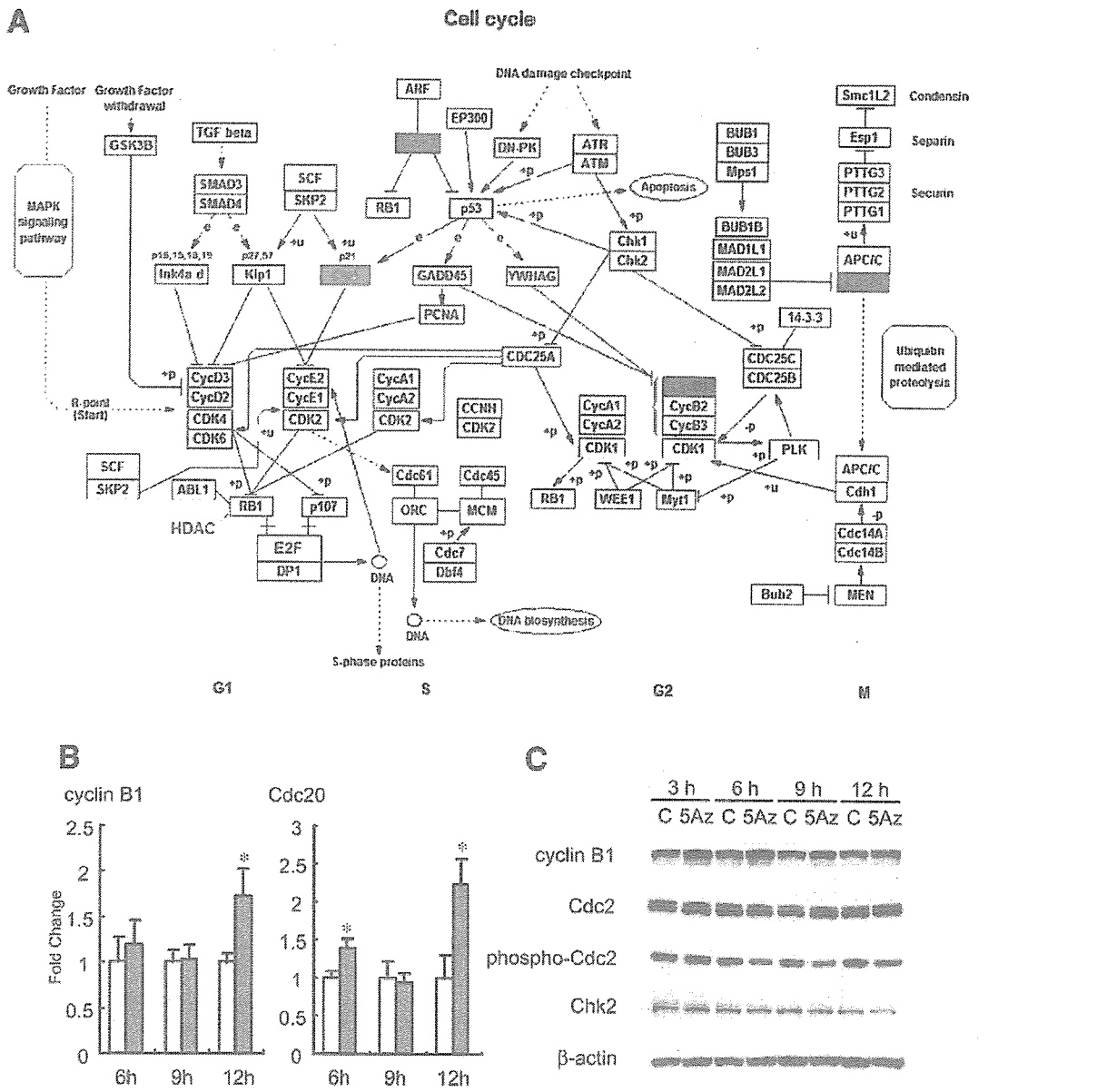

Fig. 6. Changes in the expression of G2/M phase regulators in 5AzC-treated rat fetal telencephalon. (A) The cascade of cell cycle regulation showed by GenMAPP. Red labeled genes are the upregulated genes by 5AzC treatment. They are p53-related genes ($p21^{waf1/cip1}$ and *Mdm2*) and G2/M regulating genes (*cyclin B1* and *Cdc20*). On the other hand, there are no downregulated genes. (B) mRNA expression of G2/M regulating genes, *cyclin B1* and *Cdc20*, were examined by real-time PCR. The expression of both genes was upregulated at 12 h. $^*P < 0.05$; significantly different from the control group (Student's *t* test). (C) Western blot analysis of G2/M phase regulators of control (C) and 5AzC-treated (5Az) rat fetal telencephalon. The expression of cyclin B1 increased slightly from 3 to 9 h and that of phosphorylated Cdc2 (Tyr16) decreased from 6 to 12 h, suggesting the abnormal activation of G2 to M transition. The expression and mobility of Chk2 did not change through the experimental period.

are activated in response to DNA damage (Chaturvedi et al., 1999; Liu et al., 2000; Matsuoka et al., 2000) and lead to G2 arrest through inactivation of Cdc2. The Cdc2–cyclin B complex becomes inactive after phosphorylation of tyrosine 15 and threonine 14 of Cdc2. Cdc25 dephosphorylates and activates Cdc2, but Chk1 and Chk2 phosphorylate and sequester Cdc25 in the cytoplasm, where it is ineffective. As a result, Cdc2 becomes phosphorylated and inactive. In some G2 arrest models, the arrest is reported to be brought about by Chk1 or Chk2, independent of p53 (Taylor and Stark, 2001; Iliakis et al., 2003).

However, in the present study, phospho-Cdc2 decreased, although G2 progression was blocked (Fig. 6C). This abnormal activation of Cdc2 might accelerate the G2 to M transition, probably resulting in accumulation of mitotic cells. Furthermore, the expression of cyclin B1 was slightly increased at 3 to 9 h (Fig. 6C). Cyclin B1 is degraded by anaphase-promoting complex (APC) at metaphase, and this process is indispensable for mitotic progression, so the accumulation of cyclin B1 that we observed might occur as a result of inactivation of APC, which leads to mitotic arrest (Nitta et al., 2004). The mitotic

cells we have observed have abnormal morphologies, such as dispersed chromatin and intact nuclear membranes (Ueno et al., 2002b). Recently, mitotic catastrophe, a type of cell death occurring during or after mitosis with some mitotic failure, has been proposed (Castedo et al., 2004). Although the definition of this cell death yet differs among researchers, 5AzC-induced abnormal mitosis and subsequent apoptosis might fall into this category. Indeed, aberrant entry into mitosis after DNA damage, gene deficiencies, or excess activation of Cdc2-cyclin B1 each suffices to cause mitotic catastrophe (Castedo et al., 2004), which is consistent with our model that includes DNA damage and Cdc2 activation. We should further investigate whether these mitotic cells with abnormal morphology produce two daughter cells with diploid DNA or generate tetraploid G1 cells by mitotic failure; although the results from the BrdU incorporation assay suggest that some of the cells can produce diploid cells (Fig. 3). Regardless, at 9 to 12 h, the amount of activated Cdc2 increased compared with that at 6 h (Fig. 6C), and the number of mitotic cells gradually decreased (Fig. 1B). This pattern suggests that abnormal mitotic entry is suppressed and G2-phase block is induced, although the expression level and phosphorylation state of Chk2, the regulator of the G2 checkpoint after DNA damage, did not change (Fig. 6C). Serum-inducible kinase (Snk/Plk2), which is induced by p53, likely is an inhibitor of mitotic catastrophe (Burns et al., 2003). In our microarray study, we could detect upregulated expression of *Snk/Plk2* at 9 h, when abnormal mitosis began to decrease (Table 1). The mechanism of the G2-phase block is still obscure, but from the study in p53-deficient mice, a p53-independent mechanism may be involved.

Our previous and present results reveal several clues regarding cell cycle and cell death regulation of neural progenitor cells in response to 5AzC-induced stresses, which normally proliferate with a characteristic migration–interkinetic nuclear migration (or "elevator movement")–in the VZ (Takahashi et al., 1995; Fujita, 2003; Fig. 7). Firstly M and secondly G2 progression was blocked from 6 to 9 h after 5AzC treatment and was released thereafter. Delay in inward-migration and accumulation of mitotic cells along the ventricle also were observed (Ueno et al., 2002a,b), which would reflect the delay in cell cycle progression at G2 and M phase. Then, the number of cells in G1 phase and that of apoptotic cells increased. Apoptotic cell death in a p53-dependent way occurred mainly during G1, but also during G2/M and S phase in lesser amounts. Our findings suggest that 5AzC induces apoptosis at multiple cell cycle stages, consistent with the results of another report (Murakami et al., 1995). Together, these results suggest that some cells pass from G2/M to G1 phase with completion of correct DNA repair, others enter G1 but undergo apoptosis because of incomplete repair, and still others stay in G2/M to undergo apoptotic cell death. The upregulated expression of *cyclin B1* and *Cdc20* mRNA at 12 h also suggests that the G2 block was released, and those cells entered G0/G1 phase. The cells dying at G1 after mitosis might have died due to mitotic catastrophe, as a result of incomplete mitosis and faulty DNA repair at G2 or S phase.

Because neural progenitor cells have a high proliferating activity, they are susceptible to many extrinsic stimuli,

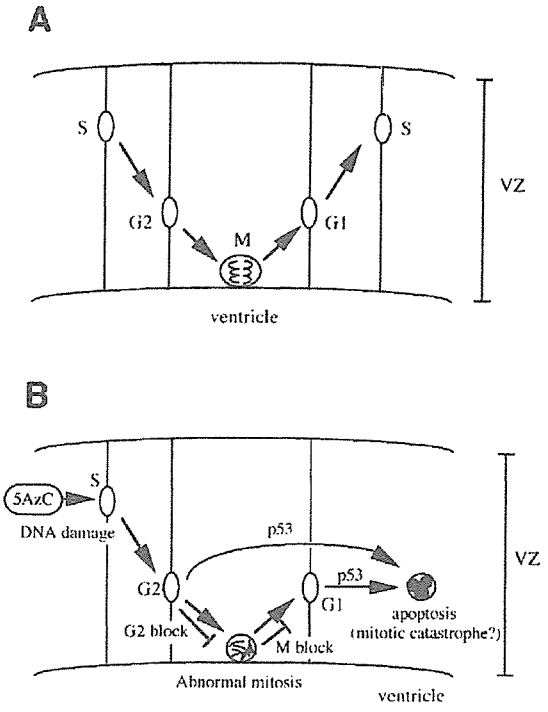

Fig. 7. 5AzC-induced alterations in proliferation of neural progenitor cells. (A) Interkinetic nuclear migration (elevator movement) of neural progenitor cells. Neural progenitor cells proliferate with their nuclei migrating up and down in the VZ. The positions of nuclei are correlated with the cell cycle phases. (B) The schema of the mechanisms of 5AzC-induced cell cycle alteration and apoptosis. 5AzC would be incorporated into DNA in S phase and cause DNA damage. Damaged neural progenitor cells enter M phase with abnormal regulation, such as excess Cdc2 activation, and they accumulate with abnormal morphologies along the ventricle. G2 block also occurs with delay in inward-migration (Ueno et al., 2002a). Then, the cells are divided into daughter cells but undergo apoptosis in G1 phase. G2 phase cells also die by apoptosis. Cell death is induced in a p53-dependent mechanism, but the G2/M phase regulation in a p53-independent way.

especially DNA damage. These cells have the potential to repair after these damages via block of cell cycle progression (or cell cycle arrest) and to exclude highly affected cells through the apoptotic process, although the responses of the cells differ slightly depending on the type of DNA damages. For example, ionizing irradiation induces G1 arrest and apoptosis in neural progenitor cells (Semont et al., 2004), whereas ethylnitrosourea induces S-phase accumulation and apoptosis (Katayama et al., 2005). Regardless, if the adverse extrinsic stimulus is sufficiently low to preclude DNA damage or allow its repair, neural progenitor cells can re-engage and proliferate for correct development of the brain after the injury. However, if the stimulus and subsequent DNA damage are high, excess cell death and cell cycle arrest occur. Thus, once the balance between proliferation and cell death is highly disturbed, it leads to abnormal brain development and results in malformation of the neonatal brain.

Many environmental stresses have a potential to disturb the processes of brain development, i.e. proliferation, migration, and differentiation, however, their mechanisms remain unclear (Rodier, 1995; Mendola et al., 2002; Costa et al., 2004). The

present study revealed how neural cells in the developing brain respond to extrinsic stimuli regarding proliferation and cell death, which offers important information to the mechanisms of fetal brain toxicity induced by widespread environmental stresses. We must further investigate the system the fetal brain uses to repair this damage and the reaction of neural progenitor cells during the repair process.

Acknowledgment

This study was supported financially by the Japan Society for the Promotion of Science.

References

Blaschke, A.J., Staley, K., Chun, J., 1996. Widespread programmed cell death in proliferative and postmitotic regions of the fetal cerebral cortex. Development 122, 1165–1174.

Burns, T.F., Fei, P., Scata, K.A., Dicker, D.T., El-Deiry, W.S., 2003. Silencing of the novel p53 target gene Snk/Plk2 leads to mitotic catastrophe in paclitaxel (taxol)-exposed cells. Mol. Cell. Biol. 23, 5556–5571.

Castedo, M., Perfettini, J.L., Roumier, T., Andreau, K., Medema, R., Kroemer, G., 2004. Cell death by mitotic catastrophe: a molecular definition. Oncogene 23, 2825–2837.

Chaturvedi, P., Eng, W.K., Zhu, Y., Mattern, M.R., Mishra, R., Hurle, M.R., Zhang, X., Annan, R.S., Lu, Q., Faucette, L.F., Scott, G.F., Li, X., Carr, S.A., Johnson, R.K., Winkler, J.D., Zhou, B.B., 1999. Mammalian Chk2 is a downstream effector of the ATM-dependent DNA damage checkpoint pathway. Oncogene 18, 4047–4054.

Costa, L.G., Aschner, M., Vitalone, A., Syversen, T., Soldin, O.P., 2004. Developmental neuropathology of environmental agents. Annu. Rev. Pharmacol. Toxicol. 44, 87–110.

D'Sa, C., Klocke, B.J., Cecconi, F., Lindsten, T., Thompson, C.B., Korsmeyer, S.J., Flavell, R.A., Roth, K.A., 2003. Caspase regulation of genotoxin-induced neural precursor cell death. J. Neurosci. Res. 74, 435–445.

D'Sa-Eipper, C., Roth, K.A., 2000. Caspase regulation of neuronal progenitor cell apoptosis. Dev. Neurosci. 22, 116–124.

Ferguson, A.T., Vertino, P.M., Spitzner, J.R., Baylin, S.B., Muller, M.T., Davidson, N.E., 1997. Role of estrogen receptor gene demethylation and DNA methyltransferase. DNA adduct formation in 5-aza-2′deoxycytidine-induced cytotoxicity in human breast cancer cells. J. Biol. Chem. 272, 32260–32266.

Fujita, S., 2003. The discovery of the matrix cell, the identification of the multipotent neural stem cell and the development of the central nervous system. Cell Struct. Funct. 28, 205–228.

Gao, Y., Sun, Y., Frank, K.M., Dikkes, P., Fujiwara, Y., Seidl, K.J., Sekiguchi, J.M., Rathbun, G.A., Swat, W., Wang, J., Bronson, R.T., Malynn, B.A., Bryans, M., Zhu, C., Chaudhuri, J., Davidson, L., Ferrini, R., Stamato, T., Orkin, S.H., Greenberg, M.E., Alt, F.W., 1998. A critical role for DNA end-joining proteins in both lymphogenesis and neurogenesis. Cell 95, 891–902.

Gorczyca, W., Gong, J., Darzynkiewicz, Z., 1993. Detection of DNA strand breaks in individual apoptotic cells by the in situ terminal deoxynucleotidyl transferase and nick translation assays. Cancer Res. 53, 1945–1951.

Iliakis, G., Wang, Y., Guan, J., Wang, H., 2003. DNA damage checkpoint control in cells exposed to ionizing radiation. Oncogene 22, 5834–5847.

Jackson-Grusby, L., Beard, C., Possemato, R., Tudor, M., Fambrough, D., Csankovszki, G., Dausman, J., Lee, P., Wilson, C., Lander, E., Jaenisch, R., 2001. Loss of genomic methylation causes p53-dependent apoptosis and epigenetic deregulation. Nat. Genet. 27, 31–39.

Juttermann, R., Li, E., Jaenisch, R., 1994. Toxicity of 5-aza-2′-deoxycytidine to mammalian cells is mediated primarily by covalent trapping of DNA methyltransferase rather than DNA demethylation. Proc. Natl. Acad. Sci. U. S. A. 91, 11797–11801.

Karpf, A.R., Moore, B.C., Ririe, T.O., Jones, D.A., 2001. Activation of the p53 DNA damage response pathway after inhibition of DNA methyltransferase by 5-aza-2′-deoxycytidine. Mol. Pharmacol. 59, 751–757.

Katayama, K., Ueno, M., Yamauchi, H., Nagata, T., Nakayama, H., Doi, K., 2005. Ethylnitrosourea induces neural progenitor cell apoptosis after S-phase accumulation in a p53-dependent manner. Neurobiol. Dis. 18, 218–225.

Keramaris, E., Stefanis, L., MacLaurin, J., Harada, N., Takaku, K., Ishikawa, T., Taketo, M.M., Robertson, G.S., Nicholson, D.W., Slack, R.S., Park, D.S., 2000. Involvement of caspase 3 in apoptotic death of cortical neurons evoked by DNA damage. Mol. Cell. Neurosci. 15, 368–379.

Kuida, K., Zheng, T.S., Na, S., Kuan, C., Yang, D., Karasuyama, H., Rakic, P., Flavell, R.A., 1996. Decreased apoptosis in the brain and premature lethality in CPP32-deficient mice. Nature 384, 368–372.

Lakin, N.D., Jackson, S.P., 1999. Regulation of p53 in response to DNA damage. Oncogene 18, 7644–7655.

Liu, Q., Guntuku, S., Cui, X.S., Matsuoka, S., Cortez, D., Tamai, K., Luo, G., Carattini-Rivera, S., DeMayo, F., Bradley, A., Donehower, L.A., Elledge, S.J., 2000. Chk1 is an essential kinase that is regulated by Atr and required for the G(2)/M DNA damage checkpoint. Genes Dev. 14, 1448–1459.

Lu, D.P., Nakayama, H., Shinozuka, J., Uetsuka, K., Taki, R., Doi, K., 1998. 5-Azacytidine-induced apoptosis in the central nervous system of developing rat fetuses. J. Toxicol. Pathol. 11, 133–136.

Matsuoka, S., Rotman, G., Ogawa, A., Shiloh, Y., Tamai, K., Elledge, S.J., 2000. Ataxia telangiectasia-mutated phosphorylates Chk2 in vivo and in vitro. Proc. Natl. Acad. Sci. U. S. A. 97, 10389–10394.

May, P., May, E., 1999. Twenty years of p53 research: structural and functional aspects of the p53 protein. Oncogene 18, 7621–7636.

Mendola, P., Selevan, S.G., Gutter, S., Rice, D., 2002. Environmental factors associated with a spectrum of neurodevelopmental deficits. Ment. Retard. Dev. Disabil. Res. Rev. 8, 188–197.

Michalowsky, L.A., Jones, P.A., 1987. Differential nuclear protein binding to 5-azacytosine-containing DNA as a potential mechanism for 5-aza-2′-deoxycytidine resistance. Mol. Cell. Biol. 7, 3076–3083.

Murakami, T., Li, X., Gong, J., Bhatia, U., Traganos, F., Darzynkiewicz, Z., 1995. Induction of apoptosis by 5-azacytidine: drug concentration-dependent differences in cell cycle specificity. Cancer Res. 55, 3093–3098.

Namihira, M., Nakashima, K., Taga, T., 2004. Developmental stage dependent regulation of DNA methylation and chromatin modification in a immature astrocyte specific gene promoter. FEBS Lett. 572, 184–188.

Nitta, M., Kobayashi, O., Honda, S., Hirota, T., Kuninaka, S., Marumoto, T., Ushio, Y., Saya, H., 2004. Spindle checkpoint function is required for mitotic catastrophe induced by DNA-damaging agents. Oncogene 23, 6548–6558.

Oppenheim, R.W., 1991. Cell death during development of the nervous system. Annu. Rev. Neurosci. 14, 453–501.

Qian, X., Shen, Q., Goderie, S.K., He, W., Capela, A., Davis, A.A., Temple, S., 2000. Timing of CNS cell generation: a programmed sequence of neuron and glial cell production from isolated murine cortical stem cells. Neuron 28, 69–80.

Rao, M.S., 1999. Multipotent and restricted precursors in the central nervous system. Anat. Rec. 257, 137–148.

Rodier, P.M., 1995. Developing brain as a target of toxicity. Environ. Health Perspect. 103, 73–76.

Santi, D.V., Norment, A., Garrett, C.E., 1984. Covalent bond formation between a DNA-cytosine methyltransferase and DNA containing 5-azacytosine. Proc. Natl. Acad. Sci. U. S. A. 81, 6993–6997.

Semont, A., Nowak, E.B., Silva Lages, C., Mathieu, C., Mouthon, M.A., May, E., Allemand, I., Millet, P., Boussin, F.D., 2004. Involvement of p53 and Fas/CD95 in murine neural progenitor cell response to ionizing irradiation. Oncogene 13, 1–12.

Sun, Y.E., Martinowich, K., Ge, W., 2003. Making and repairing the mammalian brain-signaling toward neurogenesis and gliogenesis. Semin. Cell Dev. Biol. 14, 161–168.

Takahashi, T., Nowakowski, R.S., Caviness Jr., 1995. The cell cycle of the pseudostratified ventricular epithelium of the embryonic murine cerebral wall. J. Neurosci. 15, 6046–6057.

Takizawa, T., Nakashima, K., Namihira, M., Ochiai, W., Uemura, A., Yanagisawa, M., Fujita, N., Nakao, M., Taga, T., 2001. DNA methylation is a critical cell-intrinsic determinant of astrocyte differentiation in the fetal brain. Dev. Cell 1, 749–758.

Taylor, W.R., Stark, G.R., 2001. Regulation of the G2/M transition by p53. Oncogene 20, 1803–1815.

Temple, S., 2001. The development of neural stem cells. Nature 414, 112–117.

Thomaidou, D., Mione, M.C., Cavanagh, J.F., Parnavelas, J.G., 1997. Apoptosis and its relation to the cell cycle in the developing cerebral cortex. J. Neurosci. 17, 1075–1085.

Timme, T.L., Thompson, T.C., 1994. Rapid allelotype analysis of p53 knockout mice. Biotechniques 17 (460), 462–463.

Ueno, M., Katayama, K., Nakayama, H., Doi, K., 2002a. Mechanisms of 5-azacytidine (5AzC)-induced toxicity in the rat foetal brain. Int. J. Exp. Pathol. 83, 139–150.

Ueno, M., Katayama, K., Yasoshima, A., Nakayama, H., Doi, K., 2002b. 5-azacytidine (5AzC)-induced histopathological changes in the central nervous system of rat fetuses. Exp. Toxicol. Pathol. 54, 91–96.

Vinson, R.K., Hales, B.F., 2002. DNA repair during organogenesis. Mutat. Res. 509, 79–91.

von Waechter, R., Jaensch, B., 1972. Generation times of the matrix cells during embryonic brain development: an autoradiographic study in rats. Brain Res. 46, 235–250.

Zhu, W.G., Hileman, T., Ke, Y., Wang, P., Lu, S., Duan, W., Dai, Z., Tong, T., Villalona-Calero, M.A., Plass, C., Otterson, G.A., 2004. 5-Aza-2′-deoxycytidine activates the p53/p21Waf1/Cip1 pathway to inhibit cell proliferation. J. Biol. Chem. 279, 15161–15166.

Available online at www.sciencedirect.com
SCIENCE DIRECT
Neurotoxicology and Teratology 28 (2006) 125 – 134
NEUROTOXICOLOGY AND TERATOLOGY
www.elsevier.com/locate/neutera

Molecular mechanisms of hydroxyurea(HU)-induced apoptosis in the mouse fetal brain

G.H. Woo [a], E.J. Bak [b], H. Nakayama [a], K. Doi [a,*]

[a] *Department of Veterinary Pathology, Graduate School of Agricultural and Life Sciences, The University of Tokyo, 1-1-1 Yayoi, Bunkyo-ku, Tokyo 113-8657, Japan*
[b] *Department of Biomedical Science, Graduate School of Agricultural and Life Sciences, The University of Tokyo, Japan*

Received 8 March 2005; received in revised form 26 July 2005; accepted 4 August 2005
Available online 13 December 2005

Abstract

Hydroxyurea (HU), a potent mammalian teratogen, affects proliferating embryonic cells and inhibits DNA synthesis. The teratogenic potential of HU has been well known in experimental animals for several decades. In this study, we investigated molecular mechanisms of HU-induced apoptosis in the telencephalon of the fetal brain by exposing pregnant mice to HU on day 13 of gestation. The number of TUNEL-positive cells began to increase at 3 h, peaked at 12 h, and rapidly decreased at 24 h. Although changes of *p53* mRNA expression were not observed by RT-PCR, a p53-positive reaction was detected immunohistochemically in the nuclei of neuroepithelial cells from 1 h to 6 h, and p53-protein expression was simultaneously identified by Western blot analysis. The expression of p53-target genes was detected at both the mRNA and protein. The mRNA levels of apotosis-related genes (*fas*, *fasL*, and *bax*) and cell cycle-related genes (*mdm2* and *p21*) were significantly elevated, and the degree to and sequence in which these target genes expressed was similar to those for fas, fasL, mdm2 and p21. Flow-cytometric and Western blot analyses of cell cycle-related proteins suggested that neuroepithelial cells are arrested at the S checkpoint from 3 to 6 h and at the G2/M checkpoint at 12 h, respectively. HU-induced apoptosis is considered to be mediated by p53 in the fetal brain.

Keywords: Apoptosis; p53; Cell arrest; Hydroxyurea; Fetus; Mouse

1. Introduction

Apoptosis is involved in developmental phenomena and processes such as sculpting structures, deleting unneeded structures and eliminating abnormal, misplaced, non-functional or harmful cells. It occurs as early as the blastocyst stage of development, during the formation of extraembryonic tissues, and continues throughout organogenesis [15]. It is important to emphasize that an association between excessive apoptosis and maldevelopment was observed in embryos exposed to detrimental stimuli at both pre-and post-implantation stages of development. We observed the largest cluster of TUNEL-positive nuclei in the neuroepithelium of the central nervous system (CNS) and mesenchymal cells in the lung, craniofacial tissues and limb buds of fetuses obtained from pregnant mice administrated with hydroxyurea (HU) on day 13 of gestation [39].

p53 can be activated by DNA damage, hypoxia, or aberrant oncogene expression to promote progression through cell-cycle checkpoints, DNA repair, cellular senescence, and apoptosis. Numerous studies have indicated that p53 plays a key role in apoptotic cell death following certain types of toxic stress [18,22,36,37]. Active p53 functions as a transcriptional transactivator and transrepressor, and contributes to a variety of protein–protein interactions [26]. Cell cycle arrest mediated by p53 is clearly correlated with the function of p53 as a transcriptional transactivator of genes, such as those for p21 and a cyclin-dependent kinase inhibitor.

HU is a well-known experimental teratogen and ultimately induces apoptotic cell death by a specific inhibition of DNA synthesis without any effect on RNA or protein synthesis [41]. In this study, the sequential changes in the expression of a p53-transcriptional transactivator and transrepressor were investigated in order to elucidate the molecular regulatory mechan-

* Corresponding author. Tel./fax: +81 3 5841 8185.
E-mail address: akunio@mail.ecc.u-tokyo.ac.jp (K. Doi).

0892-0362/$ - see front matter © 2005 Elsevier Inc. All rights reserved.
doi:10.1016/j.ntt.2005.08.002

isms of HU-induced apoptosis in the fetal brain. The protocol of the present study was approved by the Animal Use and Care Committee of the Graduate School of Agricultural and Life Sciences, the University of Tokyo.

2. Methods

2.1. Animals

Eighty-four 8-week-old pregnant mice of the Crj:CD-1(ICR) strain were obtained from Charles River Japan Co., Yokohama, Japan. They were kept in an animal room under controlled conditions (temperature, 23±2 °C; relative humidity, 55±5%) using an isolator caging system (Niki Shoji, Co., Tokyo) and were fed commercial pellets (MF, Oriental Yeast Co., Tokyo) and water ad libitum.

2.2. Chemicals

Hydroxyurea (HU) (Sigma, St. Louis, MO) was dissolved in distilled water immediately before use, and adjusted to a concentration of 60 mg/ml. BrdU (Sigma, St. Louis, MO) was also dissolved in physiologic saline immediately before use, at a concentration of 4 mg/ml.

2.3. Treatments

Forty-eight pregnant mice were injected with 400 mg/kg b.w. of HU intraperitoneally (i.p.) at day 13 of gestation (date vaginal plug found=day 0), and 8 dams each were sacrificed by heart puncture under ether anesthesia at 1, 3, 6, 12, 24, and 48 h after the treatment (h). Another thirty-six pregnant mice were injected i.p. with distilled water (DW), and six dams each were sacrificed in the same way. BrdU at 20 mg/kg b.w. was injected i.p. into 8 dams at each time point as well as 3 dams as controls for histopathology, immunohistochemistry and RT-PCR at 1 h before necropsy, and simultaneously with HU into 6 dams at each time point along with 3 dams as controls for Western blotting and flow cytometry.

2.4. Histopathology

Fetuses were collected by Caesarian section and fixed in 10% neutral-buffered formalin. Paraffin sections (4 μm) were stained with hematoxylin and eosin (HE). Some of the paraffin sections were subjected to immunohistochemical staining for TUNEL, p53, cleaved caspase 3 and BrdU as mentioned below.

2.5. In situ detection of fragmented DNA

DNA fragmentation was examined in the paraffin sections using the modified TUNEL method first proposed by Gravieli et al. [11], with a commercial kit (ApopTag In situ Apoptosis Detection Kit; Oncor, Gaithersburg, MD). In brief, the procedure was as follows: multiple fragmented 3′-OH ends were labeled with digoxigenin-dUTP in the presence of terminal deoxynucleotidyl transferase (TdT). Peroxidase-conjugated anti-digoxigenin antibody was then reacted with the sections. Apoptotic nuclei were visualized using peroxidase-diaminobenzidine (DAB) reaction. The sections were then counterstained with methylgreen. TUNEL-positive cells in the telencephalon were counted under a light microscope (×400). A 10×10 squared grid eyepiece was used to designate the sample field (0.0625 mm^2). The total number of positive cells was recorded from 3 randomly chosen microscope fields on each telencephalon. The average number of positive cells per field was divided by a conversion factor of 0.0625 mm^2, and the number of TUNEL positive cells was calculated. The number of TUNEL-positive cells/mm^2 was expressed as the mean±standard deviation (SD) for 5 dams (5 fetuses/dam) at each point of examination.

2.6. Immunohistochemistry

Paraffin sections of fetuses were deparaffinized and hydrated in a series of descending ethanol concentrations finishing with distilled water. For the detection of p53, sections were immersed in 10 mM citrate buffer, pH 6.0, and autoclaved for 10 min at 120 °C. After washing in tris-buffered saline (TBS), endogenous peroxidase activity was quenched for 30 min in 0.3 % H_2O_2 in methanol and the sections were washed 3 times with TBS. The sections were incubated in 8% skim milk for 40 min at 37 °C to reduce non-specific staining, and then immediately with rabbit antibody against p53 (1:300; Santa Cruz) in TBS overnight at 4 °C. After washing in TBS, sections were incubated with Envision kit (Dako, Carpinteria, CA) for 30 min at room temperature (RT), and then washed in TBS. The sections were visualized using the peroxidase-DAB reaction and then counterstained with methyl green. For the detection of cleaved caspase 3, sections were immersed in 10 mM citrate buffer, pH 6.0, and autoclaved for 10 min at 120 °C. After washing in TBS, endogenous peroxidase activity was quenched for 30 min in 0.3% H_2O_2 in methanol and the sections washed 3 times with TBS. The sections were incubated in 8% skim milk for 40 min at 37 °C to reduce non-specific staining, and then immediately in rabbit antibody against cleaved caspase 3 (1:200; Cell signaling) in TBS overnight at 4 °C. After washing in TBS, sections were incubated with biotinylated antibody against rabbit IgG (1:400; Kirkegaard and Perry, Gaitherburg, MD) according to the manufacturer's instructions, then washed in TBS and incubated with streptavidine (1:300; Dako). The sections were visualized using the peroxidase-DAB reaction and then counterstained with methyl green and coverslipped. For the detection of BrdU, sections were treated with 0.1% trypsin and 0.1% calcium chloride in Tris buffer at 37 °C and 1 N HCl at RT for 30 min each. After washing in TBS, endogenous peroxidase activity was quenched for 30 min in 0.3% H_2O_2 in methanol, and the sections were washed 3 times with TBS. The sections were incubated in 8% skim milk for 40 min at 37 °C to reduce non-specific staining, and then immediately with mouse antibody against BrdU (1:100; Dako) in TBS overnight at 4 °C. After being washed in TBS, the sections were incubated with

biotinylated antibody against mouse IgG (1:400; Kirkegaard and Perry, Gaitherburg, MD) according to the manufacturer's instructions, washed in TBS, and then incubated with streptavidine (1:300; Dako).

Positive cells in the telencephalon were counted under a light microscope (×400). The number of positive cells/mm^2 was expressed as the mean±standard deviation (SD) for 5 dams (5 fetuses/dam) at each point of examination, and a statistical analysis was done with Student's *t*-test comparing the control and HU-treated groups.

2.7. Western blotting

Embryo telencephalons were microdissected from five fetuses each of 3 dams and were frozen on dry ice. Whole embryo telencephalons were pooled and lysed in a buffer containing 50 mM Tris–HCl (pH 8.0), 150 mM NaCl, 0.02% sodium azide, 0.1% SDS, 1% NP-40, 0.5% sodium deoxycholate, 1 mM PMSF, 2 μg/ml aprotinin, 2 μg/ml leupeptins, 100 mM Na_3VO_4, and 10 mM NaF. Protein concentrations in the lysates were determined using the Bio-Rad protein assay. Samples containing equal amounts of protein were separated on 10% SDS polyacrylamide gels and blotted onto nitrocellulose membranes. Membranes were blocked in TBS containing 0.1% Tween-20 and 2.5% skim milk before the addition of antibodies. The primary antibodies used were anti-p53 (1:500; Santa Cruz), anti-p21 (1:500; PharMingen), anti-fas (1:500; Santa Cruz), anti-fasL (1:500; Santa Cruz), anti-bax (1:500; Santa Cruz), anti-cyclin B1 (1:500; Santa Cruz), anti-cyclin D1 (1:500; Dako), anti-cdk4 (1:500; Santa Cruz), anti-chk2 (1:500; Santa Cruz), anti-cyclin G1 (1:500; Santa Cruz), anti-mdm2 (1:100; Santa Cruz), anti-phospho-p53-ser 15 (1:500; Cell signaling), anti-phospho-p53-ser 20 (1:500; Cell signaling), anti-phospho-cdc2 (1:500; Cell signaling), anti-phospho-Rb (1:500; Cell signaling), and anti-β-actin (1:10 000; Sigma). Horseradish peroxidase-conjugated secondary antibodies (anti-mouse or anti-rabbit; Amersham) were used at a dilution of 1:10 000. Enhanced chemiluminescence (ECL+; Amersham) was used for signal detection before exposing blots to film.

2.8. RNA extraction and RT-PCR analysis

Telencepholons of five fetal heads from each dam were pooled and total cellular RNA was extracted from each homogenized sample using the Isogen kit (Nippon Gene, Toyama, Japan). The reverse transcription (RT) reaction for synthesizing the first strand cDNA was carried out using an oligo(dT)$_{12-18}$ primer and SUPERSCRIPT™ II Rnase H$^-$ Reverse Transcriptase (Gibco, Gaithersburg, MD). PCR was performed using oligonucleotide primers sets corresponding to the cDNA sequences of p53, its transcriptional target genes (*p21, apaf-1, bax, fas, cyclin G*, and *mdm2*), *fas L*, and *glyceraldehyde-3-phosphate dehydrogenase* (*GAPDH*) (Table 1). To determine optimized PCR cycles to achieve template amplification within exponential phase in the mouse telencephalon, validation PCR experiments by setting graded cycles from 26 to 42 were preliminary performed. PCR amplifications were performed in 50 μl of reaction mixture containing 5 μl 10× PCR buffer (100 mM Tris–HCl buffer, 500 mM KCl, and 15 mM $MgCl_2$;Takara, Shiga, Japan), 5 μl dNTP (Takara), 1.25 U of Taq™, 50 pM each of sense and antisense primer, and 1 μl of cDNA. After an initial denaturation at 94 °C for 7 min, amplification was performed in a Takara PCR Thermal cycler SP (Takara) for each cycles (Table 1) under the following conditions: 1 min of denaturation at 94 °C, 2 min (fas and fasL) or 1 min (the others) of annealing at 64 °C (fas and fasL) or 58.5 °C (the others), and 3 min (fas and fasL) or 1 min (the others) of extension at 72 °C. Amplification of GAPDH mRNA was used to control the concentration of template loaded. The PCR products were electrophoretically separated in 2% agarose S (Nippon Gene) in TBE buffer (89 mM Tris–aminomethane, 89 mM Boric acid, and 10 mM EDTA). The gels were stained with ethidium bromide (Gibco). Fluorescent bands were visualized using a UV-CCD video system (EpiLight$_{UVFA1100}$; AISIN COSMOS, Tokyo, Japan) and were analyzed using an image-analysis software, Quantity One (pdi, NY). The intensity of the band relative to the GAPDH band was represented as the mean±standard error (SE). The significance of differences between the control group and HU-treated group was evaluated with Student's *t*-test or Welch's *t*-test. For all genes, PCR cycle conditions were predetermined to give amplification within the linear range using control samples.

2.9. Flow cytomery

For the assessment of sub-G1 DNA content, the cells were prepared in two fetal telencephalons, washed in PBS, and

Table 1
Oligonucleotide primers for each molecule and cycle numbers

Gene	Sense(5′–3′)	Antisense(5′–3′)	Cycle numbers
p53	GCCAGGAGACATTTTCAGGC	AACTGCACAGGGCACGTCTT	31
p21	AATCCTGGTGATGTCCGACC	GACCAATCTGCGCTTGGAGT	32
fas	GCTCAGAAGGGAAGGAGTAC	ACTGGAGGTTCTAGATTCAGG	35
fasL	TAGACAGCAGTGCCACCACTTCAT	AACTCACGGAGTTCTGCCAGTT	39
bax	TTCATCCAGGATCGAGCAGG	TGAGGACTCCAGCCACAAAGAT	30
Apaf-1	GACTGTTGGACCGTGGCATT	CCAAGCCCTCGGAATCTTTC	37
mdm2	CATCAGGATCTTGACGATGGC	GGAGAAGCTAGATTCCACACTCT	31
Cyclin G	CTTTGGCTTTGACACGGAGAC	GGAATCGTTGGGAGGTGAGTT	33
GAPDH	TGATGGGTGTGAACCACGAG	TTGAAGTCGCAGGAGACAACC	29

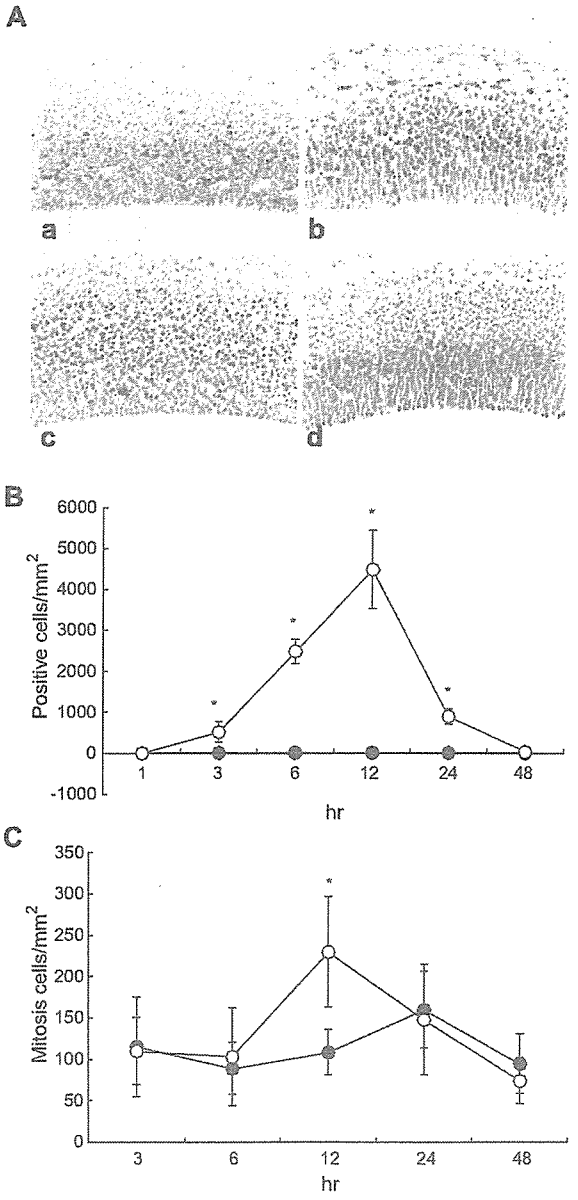

Fig. 1. Immunohistochemical staining for TUNEL. (A) TUNEL-positive cells in the telencephalon of fetuses of the HU-treated group at 3 (a), 6 (b) and 12 h (c), and of a fetus of the control group at 12 h (d). TUNEL-positive cells were mainly observed in the middle layer of the ventricular zone at 3 h, and in the middle to dorsal layers at 12 h. ×300. (B) Changes in the number of TUNEL-positive cells in the fetal telencephalon in the HU-treated (O) and control groups (●). Each value represents the mean±SD for 5 dams. The number of TUNEL-positive cells began to increase at 3 h, peaked at 12 h, and decreased at 24 h. *$p<0.01$, significantly different from the control group using Student's t-test. (C) Changes in the number of mitotic cells in the fetal telencephalon in the HU-treated (O) and control groups (●). Significant increase in the number of mitotic cells was observed in the inner layer of the ventricular zone at 12 h. See note in (B).

resuspended in 1 ml of PBS at a density of 1×10^6 cells/ml. An amount of 2.7 ml of ice-cold ethanol was added to a final ethanol concentration of 70%. After centrifugation, the cells were resuspended in 1 ml of PBS and incubated with 10 μl of RNAse for 40 min at 37 °C. An amount of 10 μl of propidium-iodide (5 mg/ml) was added. FSC and SSC analysis was performed to assess changes in cell morphology, and FL-2H analysis to detect changes in DNA content and DNA fragmentation using a FACScalibur machine (Becton-Dickson, Franklin Lakes, NJ).

For the assessment of cell cycle kinetics, the cells were fixed, washed with PBS and resuspended in 0.5% Triton X-100 in 2 N HCl for 30 min at RT. Following neutralization with 0.1 M $Na_2B_4O_7$, they were pelleted and washed with PBS. Cells were then stained with FITC-conjugated mouse anti-BrdU antibody (BD PharMingen) for 30 min in the dark at RT. They were then washed with 0.5% Tween 20 and 1% BSA in PBS, incubated with 2 μl of propidium iodide for 30 min on ice, and analyzed using the FACScalibur machine.

3. Results

3.1. Immunohistochemical findings

Results of TUNEL labeling of the fetal telencephalon are shown in Fig. 1A and B. The number of positive cells began to increase at 3 h (Fig. 1Aa), gradually increased at 6 h (Fig. 1Ab), and peaked at 12 h (Fig. 1Ac). The number of mitotic cells in the inner layer of the ventricular zone significantly increased at 12 h as compared with the control (Fig. 1C), and the change in the number of cleaved caspase 3-positive cells corresponded well to that in TUNEL-positive cells (Fig. 2). Changes in the number of p53-positive cells are shown in Fig. 3. A lot of positive cells were detected from 1 h (Fig. 3Aa) and there was no significant difference between the number at 1 h and 3 h (Fig. 3Ab). Positive cells rapidly decreased at 6 h (Fig. 3B), and returned to the control level at 12 h (Fig. 3Ac and B).

The results of BrdU labeling of the fetal telencephalon are shown in Fig. 4. The number of BrdU-positive cells significantly decreased at 3 and 12 h.

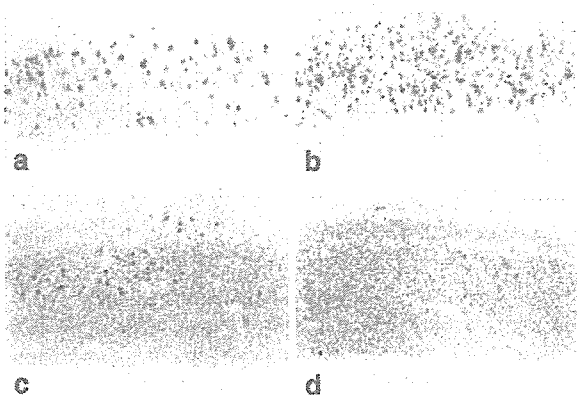

Fig. 2. Immunohistochemical staining for cleaved caspase 3 in the telencephalon of fetuses of the HU-treated group at 3 (a), 12 (b) and 24 h (c), and of a fetus of the control group at 12 h (d). The number of cleaved caspase 3-positive cells began to increase at 3 h, peaked at 12 h, and decreased at 24 h. ×300.

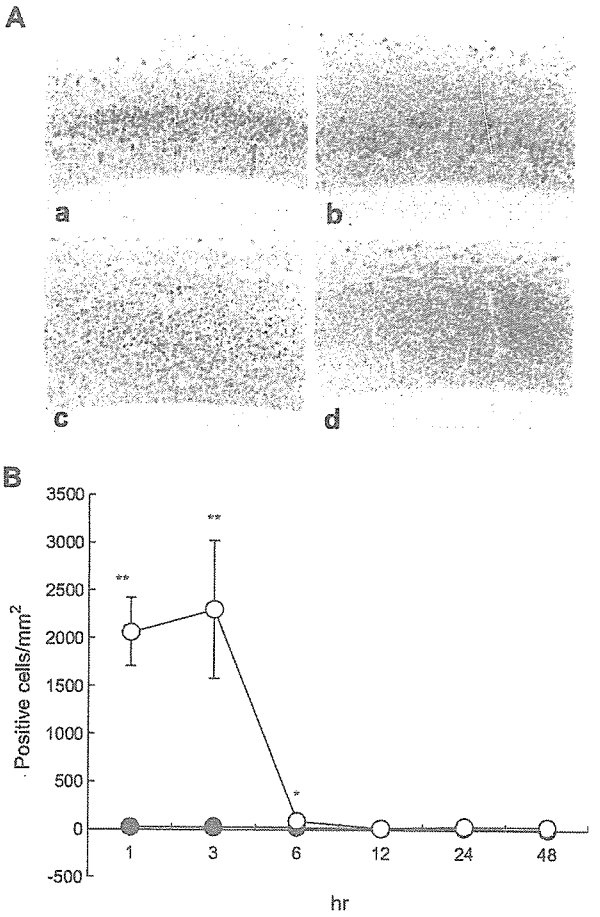

Fig. 3. Immunohistochemical staining for p53. (A) p53-positive cells in the telencephalon of fetuses of the HU-treated group at 1 (a), 3 (b) and 12 h (c), and of a fetus of the control group at 12 h (d). p53-positive cells were mainly observed in the middle layer of the ventricular zone at 1 and 3 h. ×300. (B) Changes in the number of p53-positive cells in the fetal telencephalon in the HU-treated (○) and control groups (●). Lots of p53-positive cells were observed at 1 and 3 h. p53-positive cells rapidly decreased at 6 h and returned to the control level at 12 h. Each value represents the mean±SD for 5 dams. $*p<0.05$, $**p<0.01$; significantly different from the control using Student's *t*-test.

3.2. Western blotting analysis

The results of the Western blot analysis on the expression levels of apoptosis and cell cycle arrest-related proteins (p53 and phosphorylated-p53 (Ser 15 and Ser 20), p21, bax, fas, fasL, cyclin G1, mdm2, phosphorylated-Rb, phosphorylated-cdc, cdk4, chk2, cyclin D1, and cyclin B1) in the fetal telencephalon are shown in Fig. 5.

The expression of p53 gradually increased at 12 h and decreased thereafter. Furthermore, phosphorylation of p53 at Ser 15 and Ser 20, associated with reduced interaction of p53 with mdm2, was strongly detected at 3 h. The expression of p53-transcriptional target proteins (fas, bax, cyclin G1, and p21) was seen. And fasL protein was expressed from 1 to 12 h.

The expression of mdm2 protein, a key mediator of p53 protein stability, gradually decreased to 6 h, but began to increase at 12 h.

Also, we evaluated protein expression associated with the G1/S checkpoint (cyclin D1, cdk4 and phospho-Rb) and G2/M checkpoint (cyclin B1, chk2 and phospho-cdc2). The expression of cylin D1 and cdk4 proteins decreased at 6 h. The expression of cyclin B1 protein began to decrease at 3 hr and was weakly detected at 12 h.

3.3. Findings of RT-PCR

RT-PCR analysis of the mRNA for apoptosis-associated genes in homogenates of pooled samples of the fetal telencephalon are shown in Fig. 6. The expression of *fas* mRNA significantly increased at 3–12 h as compared with that in the control group (Fig. 6). The level of *fasL* mRNA was significantly elevated from 6 h to 12 h. A significant increase in *bax* mRNA expression was also detected from 12 to 24 h (Fig. 6). The expression of *p21* mRNA showed a significantly higher level at 3 h (Fig. 6), and that of *mdm2* mRNA was significantly increased at 12 h (Fig. 6).

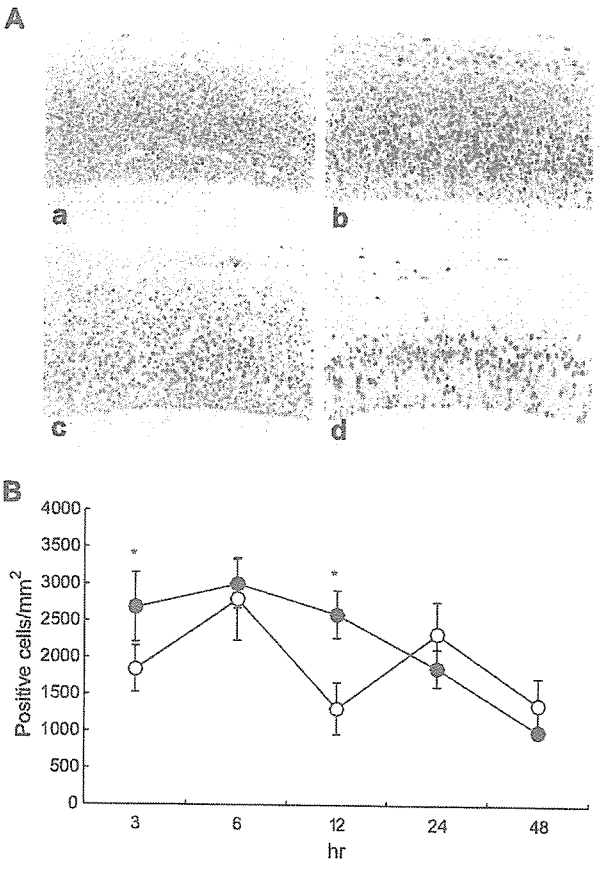

Fig. 4. Immunohistochemical staining for BrdU. (A) BrdU-positive cells in telencephalons of fetuses of the HU-treated group at 3 (a), 6 (b) and 12 h (c), and of a fetus of the control group at 6 h (d). BrdU-positive cells were mainly observed in the middle layer of the ventricular zone at all time point. ×300. (B) Changes in the number of BrdU-positive cells in the fetal telencephalon in the HU-treated (○) and control groups (●). The number of BrdU-positive cells in HU-treated group was not different from that in control group at 6 h. Each value represents the mean±SD for 5 dams. See the note in Fig. 1B.

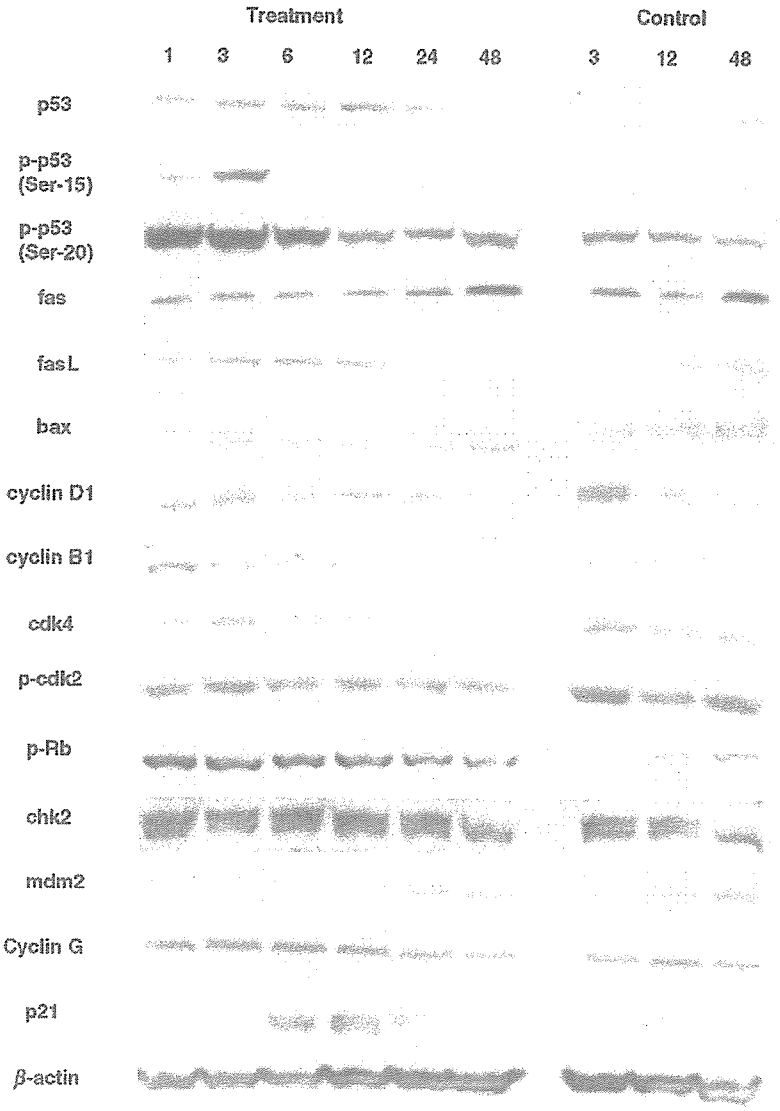

Fig. 5. Western blot analysis of the fetal telencephalon.

No significant changes were observed in the expression of *p53*, *apaf1*, and *cyclin G* mRNAs.

3.4. Flow cytometric anaysis

Flow cytometric analysis demonstrated a time-dependent appearance of DNA debris in the sub-G0/G1 region. The results corresponded well to those for pyknotic cells and TUNEL-positive cells. In addition, exposure to HU resulted in a significant and specific accumulation of cells in the S compartment and G2/M compartment of the cell cycle from 3 to 6 h and at 12 h, respectively (Fig. 7).

Fig. 8A shows the sequential changes in the number of BrdU-positive cells in the control fetal telencephalon. Most neuroepithelial cells entered the S phase after 1 h, moved to the M phase after 6 h, and returned to the G1 phase after 12 h. The results of flow cytometric analysis in the HU-treated group (Fig. 8B) were similar to those for pyknotic cells, TUNEL-positive cells, and BrdU-positive cells.

4. Discussion

It is generally recognized that HU-induced teratogenecity is due to an inhibition of DNA synthesis, which is caused by the blocking of the enzyme ribonucleotide reductase, resulting in a depletion of deoxyribonucleoside triphosphate pools [3,7]. We reported that embryonic maldevelopment was preceded by excessive apoptosis in embryonic target organs when pregnant mice were administrated with HU on day 13 of gestation [39]. In addition, in a study on the neonates and offspring from pregnant mice treated with 400 mg/kg or 800 mg/kg of HU on day 13 of gestation, we reported that the neonates and offspring from pregnant mice treated with HU were retarded in growth, and the organ weights of brain and lungs of the HU-treated

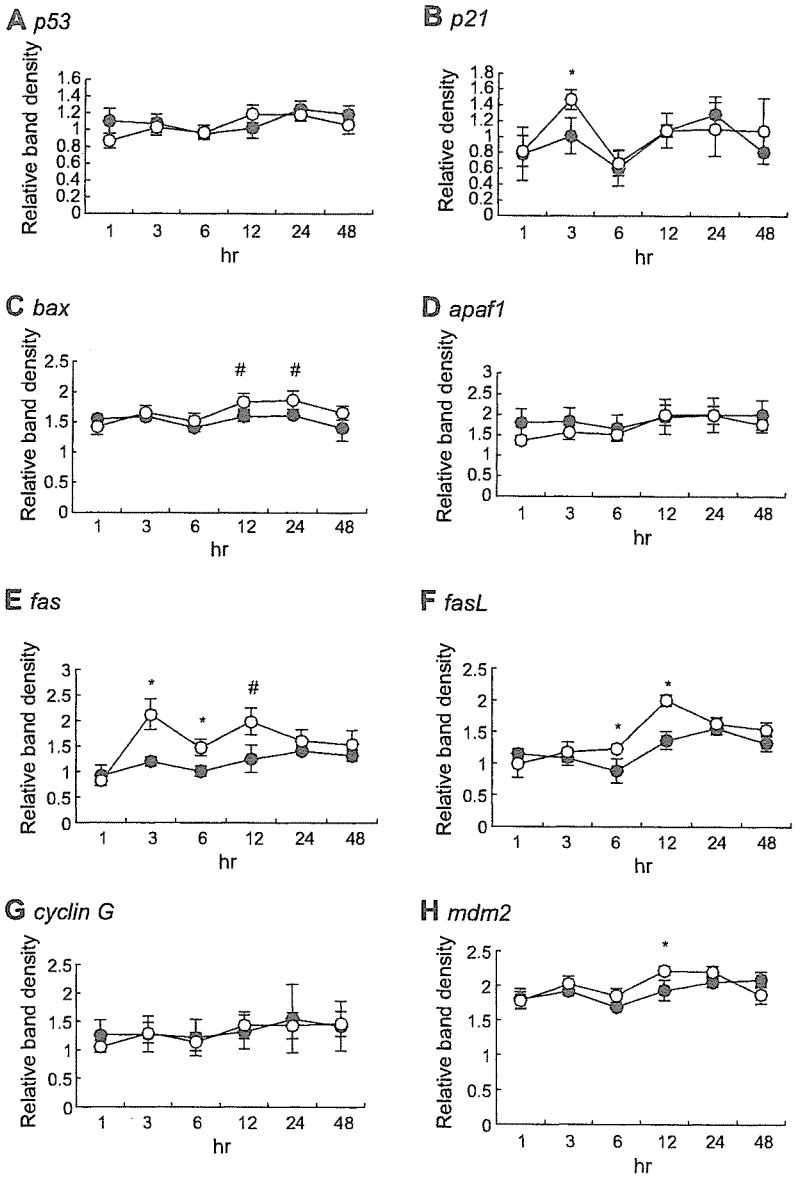

Fig. 6. RT-PCR analysis of sequential changes in the mRNA levels of p53 and its transcriptional targets. Each value represents the mean ± SE for 5 dams (HU-treated group) (○) or 3 dams (control group) (●). *$p < 0.05$ (Student's t-test), #$p < 0.05$ (Welch's t-test); Significantly different from the control.

group were significantly lower than those of the control group [40].

In the present study, the sequential changes in the expression of p53 and its transcriptional targets (*p21*, *apaf-1*, *bax*, *cyclin G*, *mdm2*, and *fas*) were examined in the fetal mouse telencephalon from dams treated with HU, because p53 is said to play an important role in the induction of apoptosis [20]. Activation of p53 in response to cytotoxic stress such as ionizing radiation [16], glutamate [36] and ischemia [6] depends to a large extent on the stabilization of p53 protein, which rapidly accumulates in stressed cells. Lots of p53-positive neuroepithelial cells were observed from 1 h in the present study, and p53 protein was strongly expressed from 1 h to 12 h. The results indicated that HU-induced apoptosis in the fetal brain was p53-dependent. Also, increases in 53 protein phosphorylated at Serine 15 and 20 were strongly detected from 1 to 6 h. Recent studies have shown that some DNA-damaging agents induce site-specific phosphorylation within the N terminus of p53, specifically at Serine 15, 20, 33, 37, and 46 [1,4,5,29,31,32]. However, no change in *p53* mRNA expression was seen in the present study. In this regard, it is reported that, although the level of *p53* mRNA does not change detectably in response to DNA damage, the level of p53 protein increases rapidly [17].

Degradation of p53 is regulated by interaction with mdm2 protein, which is itself transcriptionally regulated by p53, establishing a negative feedback loop where increased levels of p53 increase the expression of mdm2 [2,12,19]. In the

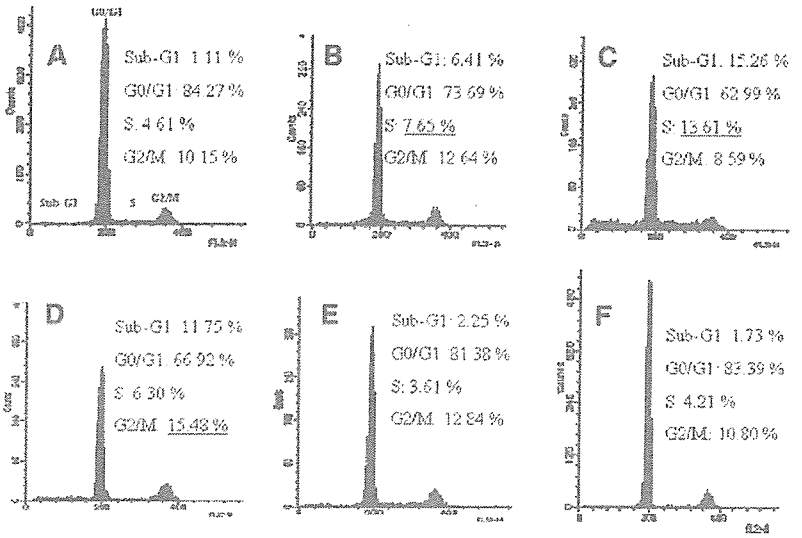

Fig. 7. Cell cycle profile in the neuroepithelial cells of fetal telencephalon at 1 (A), 3 (B), 6 (C), 12 (D) and 24 h (E) after treatment with HU, and of the control group (F). The gates for the sub-G0/G1, G0/G1, S, and G2/M phases are shown.

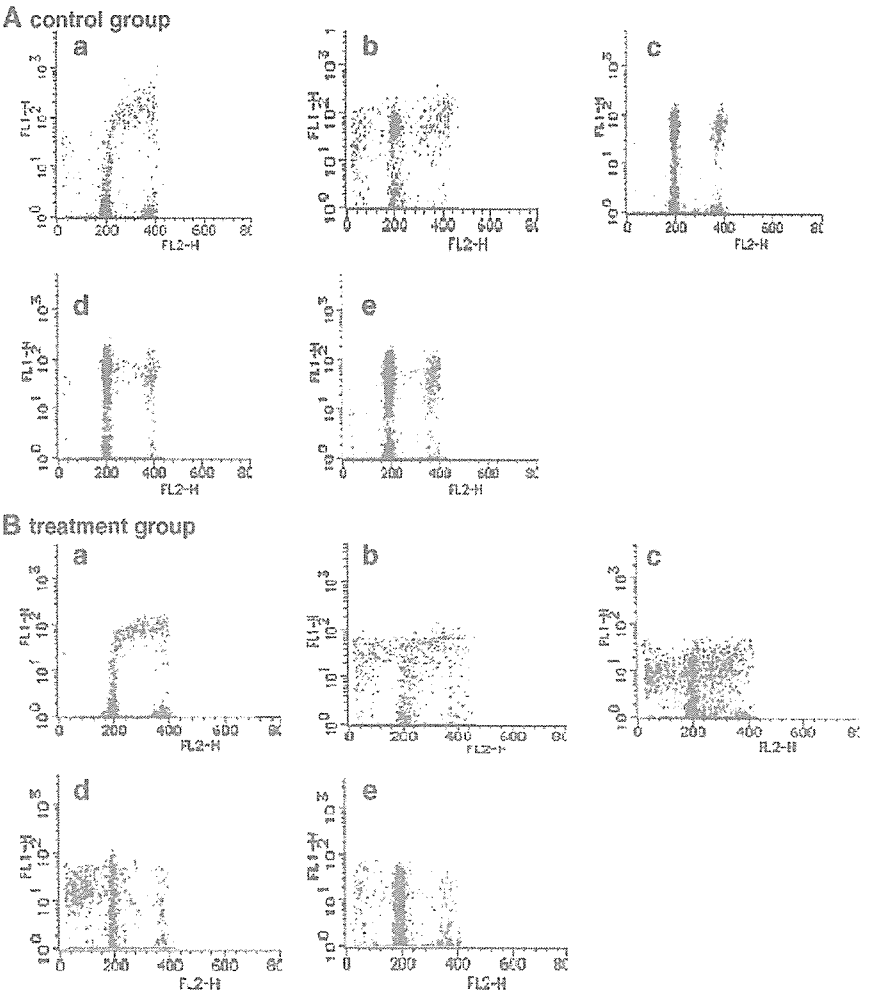

Fig. 8. Flow cytometric analysis of cellular DNA content and BrdU incorporation. (A) BrdU-positive cells in the telencephalon in the control group at 1 (a), 3 (b), 6 (c), 12 (d) and 24 h (e). (B) BrdU-positive cells in the telencephalon in the HU-treated group at 1 (a), 3 (b), 6 (c), 12 (d) and 24 h (e).

present study, the expression of p53 protein gradually increased from 1 to 12 h, and p53 phosphorylated at serines 15 and 20 disappeared or its level was reduced from 12 h. On the other hand, mdm2 protein began to increase at 12 h. Phosphorylation at serines 15 and 37 or at serine 20 was said to reduce the interaction between p53 and mdm2 in vitro [30,38].

p53-induced apoptosis is proposed to be mediated by the transactivation of bax [21], fas/APO1 [24] and p53-inducible genes [25]. Although the timing of the expression of bax protein was not consistent with that of *bax* mRNA, a significant change of bax protein and the mRNA expression was seen in the present study. Early cell changes that occur during apoptosis are associated with mitochondrial changes mediated by the bcl-2 families of proteins, including anti-apoptotic bcl-2 and pro-apoptotic bax proteins [35]. Bax expression is upregulated during p53-dependent apoptosis[21]. Bax accelerates the release of the apoptosis-inducing factor and cytochrome *c* from the mitochondria, thus activating the caspase cascade [33]. In addition, caspase activation was identified by immunochemistry for cleaved caspase 3.

Significant changes in the expression of *fas* and *fasL* mRNAs as well as their proteins were observed in the present study. This suggests an important role for the fas/CD95-fasL receptor-ligand system in HU-induced apoptosis. Fas is induced by p53 in response to genotoxic damaging agents and it is said that fas is necessary for T cell-mediated apoptosis after treatment with anticancer drugs [10,33]. Tumor cells expressing wt p53 are more sensitive to drug-induced apoptosis mediated by fas-dependent signals [23].

In the present study, a significant increase in *p21* mRNA expression appeared at 3 h. An elevation of *p21* mRNA expression was observed following p53 protein expression. Also, the number of BrdU-positive cells, i.e. S phase cells, returned to the level found in the control group at 6 h. In addition, the number of mitotic cells in the inner layer of the ventricular layer significantly increased at 12 h. These findings suggest that HU induces cell arrest. In the flow cytometric analysis, cell cycle arrest was detected at the S checkpoint from 3 to 6 h and at the G2/M checkpoint at 12 h, respectively. p21 is largely responsible for p53-dependent G1 arrest in response to radiation [8]. Negative regulation of the G1 phase cyclin/cdk complex (cyclin D1/cdk 4, 6 and cyclin E/cdk2) plays a key role in the G1/S checkpoint. Cdks are negatively regulated by cdk inhibitors such as p21. Induction and activation of p53 lead to transcriptional induction of p21 owing to strong p53 response elements in the p21 gene promoter. Then, p21 binds and inactivates cyclin D1/cdk4, 6 and cyclin E/cdk2 complexes, resulting in hypophosphorylation of RB and cell cycle arrest [35]. G2 arrest is brought about through signaling cascades that converge to inhibit the activation of cdc2 [13]. Recent study shows that p53 and p21 are necessary to maintain G2 arrest following DNA damage [9]. The mechanism of p53-dependent G2 arrest involves an initial inhibition of cyclin B1/cdc2 activation by p21 and a subsequent reduction of cyclin B1 and cdc2 protein levels [9,14].

Cyclin G1 and apaf-1 are among the targets of the transcription factor, p53. Although the function of cyclin G in the p53 pathway has not been elucidated, it has been reported that cyclin G promotes growth [27,34]. Expression of apaf-1 has been shown to be essential for the p53-dependent apoptosis induced by treatment with DNA-damaging agents [28].

In summary, the neuroepithelial cell death induced by HU may be dependent on p53. Therefore, p53 may form an important link between DNA damage by HU and neuroepithelial cell death.

References

[1] S. Banin, L. Moyal, S. Shieh, Y. Taya, C.W. Anderson, L. Chessa, N.I. Smorodinsky, C. Prives, Y. Reiss, Y. Shiloh, Y. Ziv, Enhanced phosphorylation of p53 by ATM in response to DNA damage, Science 281 (1998) 1674–1677.

[2] Y. Barak, T. Juven, R. Haffner, M. Oren, mdm2 expression is induced by wild type p53 activity, EMBO J. 12 (1993) 461–468.

[3] V. Bianchi, E. Pontis, P. Reichard, Changes of deoxyribonucleoside triphosphate pools induced by hydroxyurea and their relation to DNA synthesis, J. Biol. Chem. 261 (1986) 16037–16042.

[4] D. Bulavin, S. Sairo, M.C. Hollander, K. Sakaguchi, C.W. Anderson, E. Appella, A.J. Fornace, Phosphorylation of human p53 by p38 kinase coordinates N-terminal phosphorylation and apoptosis in response to UV radiation, EMBO J. 18 (1999) 6845–6854.

[5] C.E. Canman, D.S. Lim, K.A. Cimprich, Y. Taya, K. Tamai, K. Sakaguchi, E. Appella, M.B. Kastan, J.D. Siliciano, Activation of the ATM kinase by ionizing radiation and phosphorylation of p53, Science 281 (1998) 1677–1679.

[6] Y.H. Chung, C.M. Shin, M.J. Kim, E.Y. Lee, G. Kim, C.I. Cha, Enhanced expression of p53 in reactive astrocytes following transient focal ischemia, Neurol. Res. 24 (2002) 324–328.

[7] A. Collins, D.J. Oates, Hydroxyurea: effects on deoxyribonucleotide pool sizes correlated with effects on DNA repair in mammalian cells, Eur. J. Biochem. 169 (1987) 299–305.

[8] V. Dulic, W.K. Kaufmann, S.J. Wilson, T.D. Tlsty, E. Lees, J.W. Harper, S.J. Elledge, S.I. Reed, P53-dependent inhibition of cyclin-dependent kinase activities in human fibroblasts during radiation-induced G1 arrest, Cell 76 (1994) 1013–1023.

[9] P.M. Flatt, L.J. Tang, C.D. Scatena, S.T. Szak, J.A. Pietenpol, p53 regulation of G(2) checkpoint is retinoblastoma protein dependent, Mol. Cell Biol. 20 (2000) 4210–4223.

[10] C. Friesen, I. Herr, P.H. Krammer, K.M. Debatin, Involvement of the CD95(APO1/Fas) receptor/ligand system in drug-induced apoptosis in leukemia cells, Nat. Med. 2 (1996) 574–577.

[11] Y. Gravieli, Y. Sherman, S. Ben, Identification programmed cell death in situ via specific labeling of nuclear DNA fragmentation, J. Cell Biol. 119 (1992) 493–501.

[12] Y. Haupt, R. Maya, A. Kazaz, M. Oren, Mdm2 promotes the rapid degradation of p53, Nature 387 (1997) 296–299.

[13] A. Hwang, R.J. Muschel, Radiation and the G2 phase of the cell cycle, Radiat. Res. 150 (1998) S52–S59.

[14] S.A. Innocente, J.L. Abrahamson, J.P. Cogswell, J.M. Lee, p53 regulates a G2 checkpoint through cyclin B1, Proc. Natl. Acad. Sci. U. S. A. 96 (1999) 2147–2152.

[15] M.D. Jacobson, M. Weil, M.C. Raff, Programmed cell death in animal development, Cell 88 (1997) 347–354.

[16] J. Jordan, M.F. Galindo, J.H. Prehn, R.R. Weichselbaum, M. Beckett, G.D. Ghadge, R.P. Roos, J.M. Leiden, R.J. Miller, p53 expression induces apoptosis in hippocampal pyramidal neuron cultures, J. Neurosci. 17 (1997) 397–405.

[17] M.B. Kastan, O. Onyekwere, D. Sidransky, B. Vogelstein, R.W. Craig, Participation of p53 in the cellular response to DNA damage, Cancer Res. 51 (1991) 6304–6311.

[18] K. Katayama, K. Uetsuka, N. Ishigami, H. Nakayama, K. Doi, Apoptotic cell death and cell proliferative activity in the rat fetal central nervous system from dams administered Ethylnitrosourea(ENU), Histol. Histopathol. 16 (2001) 79–85.
[19] M.H.G. Kubbutat, S.N. Jones, K.H. Vousden, Regulation of p53 stability by Mdm2, Nature 387 (1997) 299–303.
[20] N.D. Lakin, S.P. Jackson, Regulation of p53 in response to DNA damage, Oncogene 18 (1999) 7644–7655.
[21] T. Miyashita, J.C. Reed, Tumor suppressor p53 is a direct transcriptional activator of the human bax gene, Cell 80 (1995) 293–299.
[22] J. Morrison, H.J. Wenzel, Y. Kinoshita, C.A. Robbins, L.A. Donehower, P.A. Schwartzkroin, Loss of the p53 tumor suppressor gene protects neurons from kainate-induced cell death, J. Neurosci. 16 (1996) 1337–1345.
[23] M. Muller, S. Strand, H. Hug, E.M. Heinemann, H. Walczak, W.J. Hofmann, W. Stremmel, P.H. Krammer, P.R. Galle, Drug-induced apotosis in hepatoma cells is mediated by the CD95(APO-1/Fas) receptor/ligand system and involves activation of wild-type p53, J. Clin. Invest. 99 (1997) 403–413.
[24] L.B. Owen-Scaub, W. Zhang, J.C. Cusack, L.S. Angelo, S.M. Santee, T. Fujiwara, J.A. Roth, A.B. Deisseroth, W.W. Zhang, E. Kruzel, R. Radinsky, Wild-type human p53 and a temperature-sensitive mutant induce Fas/APO-1 expression, Mol. Cell. Biol. 15 (1995) 3032–3040.
[25] K. Polyak, Y. Xia, J.L. Zweier, K.W. Kinzler, B. Vogelstein, A model for p53-induced apoptosis, Nature 389 (1997) 300–305.
[26] J. Prives, P.A. Hall, The p53 pathway, J. Pahol. 187 (1999) 112–126.
[27] C.L. Reimer, A.M. Boras, S.K. Kurdistanni, J.R. Garreau, M. Chung, S.A. Aaronson, S.W. Lee, Altered regulation of cyclin G in human breast cancer and its specific localization at replication foci in response to DNA damage in p53+/+cells, J. Biol. Chem. 274 (1999) 11022–11029.
[28] A.I. Robles, N.A. Bemmels, A.B. Foraker, C.C. Harris, A PAF-1 is a transcriptional target of p53 in DNA damage-induced apoptosis, Cancer Res. 61 (2001) 6660–6664.
[29] K. Sakaguchi, J.E. Herrera, S. Saito, T. Miki, M. Bustin, A. Vassilev, C.W. Anderson, E. Appella, DNA damage activates p53 through a phosphorylation-acetylation cascade, Genes Dev. 12 (1998) 2831–2841.
[30] S.Y. Shieh, M. Ikeda, Y. Taya, C. Prives, DNA damage-induced phosphorylation of p53 alleviates inhibition by MDM2, Cell 91 (1997) 325–334.
[31] S.Y. Shieh, Y. Taya, C. Prives, DNA damage-inducible phosphorylation of p53 at N-terminal sites including a novel site, Ser20, requires tetramerization, EMBO J. 18 (1999) 1815–1823.
[32] J.D. Siliciano, C.E. Canman, Y. Taya, K. Sakaguchi, E. Appella, M.B. Kastan, DNA damage induces phosphorylation of the amino terminus of p53, Genes Dev. 11 (1997) 3471–3481.
[33] R.V. Sionov, Y. Haupt, The cellular response to p53: the decision between life and death, Oncogene 18 (1999) 6145–6157.
[34] M.L. Smith, H.U. Kontny, R. Bortnick, A.J. Fornace Jr., The p53-regulated cyclin G gene promotes cell growth:p53 downstream effectors cyclin G and Gadd45 exert different effects on cisplatin chemosensitivity, Exp. Cell Res. 230 (1997) 61–68.
[35] Z.A. Stewart, J.A. Pietenpol, p53 signaling and cell cycle checkpoints, Chem. Res. Toxicol. 14 (2001) 243–263.
[36] D. Uberti, M. Belloni, M. Grilli, P. Spano, M. Memo, Induction of tumour-suppressor phosphoprotein p53 in the apoptosis of cultured rat cerebellar neurones triggered by excitatory amino acids, Eur. J. Neurosci. 10 (1998) 246–254.
[37] M. Ueno, K. Katayama, H. Nakayama, K. Doi, Mechanisms of 5-azacytidine(5AzC)-induced toxicity in the rat foetal brain, Int. J. Exp. Pathol. 83 (2002) 139–150.
[38] T. Unger, T. Juven-Gershon, E. Moallem, M. Berger, R. Vogt Sionov, G. Lozano, M. Oren, Y. Haupt, Critical role for Ser20 of human p53 in the negative regulation of p53 by Mdm2, EMBO J. 18 (1999) 1805–1814.
[39] G.H. Woo, K. Katayama, J.Y. Jung, K. Uetsuka, E.J. Bak, H. Nakayama, K. Doi, Hydroxyurea(HU)-induced apoptosis in the mouse fetal tissues, Histol. Histopathol. 18 (2003) 387–392.
[40] G.H. Woo, K. Katayama, E.J. Bak, M. Ueno, H. Yamauchi, K. Uetsuka, H. Nakayama, K. Doi, Effects of prenatal hydroxyurea-treatment on mouse offspring, Exp. Toxic. Pathol. 56 (2004) 1–7.
[41] J.W. Yarbro, Mechanism of action of hydroxyurea, Semin. Oncol. 19 (1992) 1–10.

J Neuropathol Exp Neurol

Vol. 65, No. 9
September 2006
pp. 873–882

ORIGINAL ARTICLE

Evidence of Apoptosis in the Subventricular Zone and Rostral Migratory Stream in the MPTP Mouse Model of Parkinson Disease

Xi Jun He, MS, Hiroyuki Nakayama, DVM, PhD, Mei Dong, MS, Hirofumi Yamauchi, DVM, MS, Masaki Ueno, DVM, PhD, Koji Uetsuka, DVM, PhD, and Kunio Doi, DVM, PhD

Abstract

1-methyl-4-phenyl-1,2,3,6-tetrahydropyridine (MPTP) is commonly used to create animal models of Parkinson disease. There is conflicting evidence on the occurrence of apoptosis induced by MPTP in the mouse substantia nigra pars compacta. We demonstrated that a single acute injection of MPTP induced apoptosis in the subventricular zone (SVZ) and rostral migratory stream (RMS) in the adult C57BL/6 mouse brain. The number of TUNEL-positive cells peaked at 24 hours after injection and decreased thereafter, paralleling the change in the number of cleaved caspase-3-positive cells after MPTP injection. Results of immunohistochemistry and ultrastructural analyses indicated that the majority of apoptotic cells in the SVZ and RMS were migrating neuroblasts (type A cells), whereas a few were astrocytes (type B cells). No apoptosis occurred in transit-amplifying progenitors (type C cells). The decrease in A cell numbers was most marked on day 2 and lasted to day 8 after the administration. A rapid and transient phagocytosis of apoptotic cells by microglial cells was demonstrated to parallel the MPTP-induced apoptosis. The present findings provide new insight into the extensive neurotoxicity of MPTP and may be valuable in reevaluating the MPTP mouse model of Parkinson disease.

Key Words: Apoptosis, Migrating neuroblast, MPTP, Parkinson disease, Rostral migratory stream, Subventricular zone.

INTRODUCTION

1-methyl-4-phenyl-1,2,3,6-tetrahydropyridine (MPTP) is a byproduct of the chemical synthesis of a meperidine analog with potent heroin-like effects (1) that causes damage to dopaminergic neurons and depletes dopamine in a manner similar to that seen in Parkinson disease (PD). When administered to animals, MPTP passes through the blood–brain barrier and is converted, mainly in glial cells, into its active form, 1-methyl-4-phenylpyridinium (MPP^+), by an enzyme, monoamine oxidase B (MAO-B) (2). For the last 2 decades, MPTP has been widely used to generate animal models of PD in rodents and nonhuman primates. A few studies have confirmed that MPTP can induce apoptosis of dopaminergic neurons in vivo (3–5). When injected intraperitoneally with a subacute regimen, which consists of one injection per day (30 mg/kg per day) for 5 consecutive days, MPTP induces dopaminergic cell loss by a mechanism mainly involving apoptosis (6). The use of this subacute regimen has been the main approach to studying the apoptosis of dopaminergic cells in mice. The induction of apoptosis in mouse nigrostriatal glia has also been demonstrated with this regimen (7), indicating that neurotoxicity of MPTP is not specifically restricted to dopaminergic neurons in the mouse brain. Furthermore, results from studies in vitro show that MPTP or MPP^+ induces apoptosis in primary cultured cerebellar granular neurons (8, 9), mesencephalic dopaminergic neurons (10), and neuroblastoma cells (11, 12) as well as PC12 cells (13, 14).

Recently, attention has been focused on the influence of MPTP on neurogenesis (15–17). Results from Hoglinger et al suggest that dopamine depletion in MPTP-treated mice and in patients with PD impairs the proliferation of neural precursor cells that express dopamine receptors and receive dopaminergic afferents (16). This demonstrated the neurotoxicity of MPTP in cells in the subventricular zone (SVZ). In the adult mouse brain, the SVZ is the largest germinal region and harbors neural stem cells that retain the capacity to generate multiple cell types (18). In adult mice, the SVZ is composed of migrating neuroblasts (type A cells), astrocytes (neural stem cells, type B cells), immature precursors (rapidly dividing transit amplifying cells, type C cells), and ependymal cells (19, 20). Type B cells divide to give rise to clusters of type C cells, which in turn generate migrating neuroblasts (type A cells) (20). Newly generated neuroblasts in the SVZ migrate along the rostral migratory stream (RMS) to enter the olfactory bulb (OB), where they differentiate into interneurons (21, 22).

The multipotential progenitor cells reside in SVZ and RMS are eliminated through apoptosis to maintain a balance for proper development of the mammalian nervous system (23–25). The mechanism of apoptotic death in the SVZ and

From the Departments of Veterinary Pathology (XJH, HN, HY, MU, KU, KD) and Veterinary Public Health (MD), Graduate School of Agricultural and Life Sciences, The University of Tokyo, Tokyo, Japan.
Send correspondence and reprint requests to: Xi Jun He, MS, Department of Veterinary Pathology, Graduate School of Agricultural and Life Sciences, The University of Tokyo, 1-1-1 Yayoi, Bunkyo-ku, Tokyo 113-8657, Japan; E-mail: aaa37172@mail.goo.ne.jp

RMS is attracting much interest and remains to be clarified. Apoptosis has been induced experimentally in the SVZ and RMS by applying extraneous insults. Hypoxia/ischemia deplete oligodendrocyte progenitors and neural stem cells in the rat perinatal SVZ through the processes of necrosis and apoptosis (26). Nitric oxide induces apoptosis of neural progenitor cells (C17.2 line) by a mechanism requiring the activation of p38 MAP kinase, poly(ADP-ribose) polymerase, and caspase-3 (27). A single intrauterine administration of ethyl-nitrosourea, a known DNA mutagen and neural carcinogen, triggered the apoptosis of neural precursor cells and activation of caspase-3 both in vivo (mouse embryos) and in vitro (28). Irradiation has also been demonstrated to induce apoptosis of SVZ cells and/or dentate gyrus progenitor cells in the rat brain (29–31). Neurogenesis occurs constitutively throughout adulthood in the SVZ and dentate gyrus, yet the rate of neurogenesis is regulated in various physiological and pathologic conditions (32). Given these findings, it is obvious that neurogenesis in adults could be impaired through the induction by extraneous factors of apoptosis in neural progenitor cells in the SVZ. In patients with PD and MPTP-treated mice, it has been shown that numbers of proliferating cells in the subependymal zone and neural precursor cells in the subgranular zone and olfactory bulb are reduced (16). Although this proved to be a result of dopamine depletion, it raises the possibility that in patients with PD and animal models of PD, the impaired neurogenesis may further delay the recovery from degeneration or cell loss in the dopaminergic system. In the present study, we have obtained evidence for the induction of apoptosis by MPTP in the SVZ and RMS in the adult mouse brain, suggesting that neurotoxicity of MPTP is not specifically restricted to dopaminergic neurons in the mouse brain, although MPTP regimen-dependent differences may also exist.

MATERIALS AND METHODS

Animals and Treatments

Three-month-old male C57BL/6 mice, weighing 25 to 30 g (Clea Japan, Tokyo, Japan), were housed in a temperature-controlled room under a 12/12-hour light/dark cycle with ad libitum access to food and water. On the day of the experiment, mice received one intraperitoneal injection of MPTP-HCl (50 mg/kg; Sigma, St. Louis, MO) dissolved in saline; control mice received saline only. MPTP-treated and control mice were killed at defined time points after the injection under deep anesthesia. All procedures used in this study were approved by the Committee of Animal Experiments, Graduate School of Agricultural and Life Science, the University of Tokyo.

Tissue Preparation

Immediately after the brains were isolated, they were fixed in 10% neutral-buffered formalin, embedded in paraffin, and cut into 4-μm coronal or sagittal sections encompassing the entire SVZ and RMS. The sections were used for TUNEL, immunohistochemistry, and immunofluorescence histochemistry as well as for staining with hematoxylin and eosin (H&E).

Immunohistochemistry

Tissue sections were used for immunohistochemistry with the following primary antibodies: goat antidoublecortin (Dcx, 1:200; Santa Cruz Biotechnology, Santa Cruz, CA) as a marker for migrating neuroblasts (type A cells); rabbit antiglial fibrillary acidic protein (GFAP, 1:100; DAKO, Carpinteria, CA) as a marker for astrocytes (type B cells); rabbit antityrosine hydroxylase (TH, 1:100; Chemicon, Temecula, CA) as dopaminergic marker; and rabbit anti-ionized calcium-binding adaptor molecule1 (Iba 1, 1:250; Wako, Osaka, Japan) as a marker for microglial cells. The binding of the biotinylated secondary antibody was detected using a LSAB method with streptavidin (1:300; DAKO). The sections were visualized using 0.05% 3,3-diaminobenzidine (DAB) with 0.03% hydrogen peroxide in Tris-HCl buffer and counterstained with methyl green.

Detection of Cleaved Caspase-3 by Immunohistochemistry

Immunohistochemistry for cleaved caspase-3 was also performed by the standard procedure described previously using rabbit anticleaved caspase-3 antibody (1:100; Cell Signaling Technology, Beverly, MA). For fluorescence immunohistochemistry, after incubation with biotinylated anti-rabbit IgG antibody, specimens were reacted with Texas Red Avidin D (1:100; Vector Laboratories, Burlingame, CA), and examined using a Zeiss LSM510 confocal laser scanning microscope.

Double-Labeling Immunofluorescence

To determine the phenotype of the cells undergoing apoptosis, double-labeling immunofluorescence histochemistry was performed using the anticleaved caspase-3 antibody and either the goat anti-Dcx or rabbit anti-GFAP antibody described previously or mouse antiepidermal growth factor receptor (EGFR, 1:50; DAKO) or mouse anti-Lewis X (LeX, clone MMA, also known as ssea-1 or CD15, 1:50; BD Bioscience, Heidelberg, Germany) as a marker for transit-amplifying precursors (type C cells). After visualization with Texas red-conjugated anti-rabbit antibody (1:100; Vector Laboratories), tissue sections were incubated with an Avidin/Biotin Blocking Kit (Vector Laboratories) and then with another primary antibody. Visualization of the cell markers was accomplished using FITC-conjugated species-specific secondary antibodies: FITC-conjugated donkey anti-goat IgG, FITC-conjugated goat anti-rabbit IgG (1:100; Santa Cruz Biotechnology), and FITC-conjugated goat anti-mouse IgG (1:100; Vector Laboratories). Sections were mounted with Vectashield (Vector Laboratories) and observed using the Zeiss LSM510 confocal laser scanning microscope.

TUNEL Method

Tissue sections were processed for fluorescence TUNEL staining by using the ApopTag Fluorescein In Situ

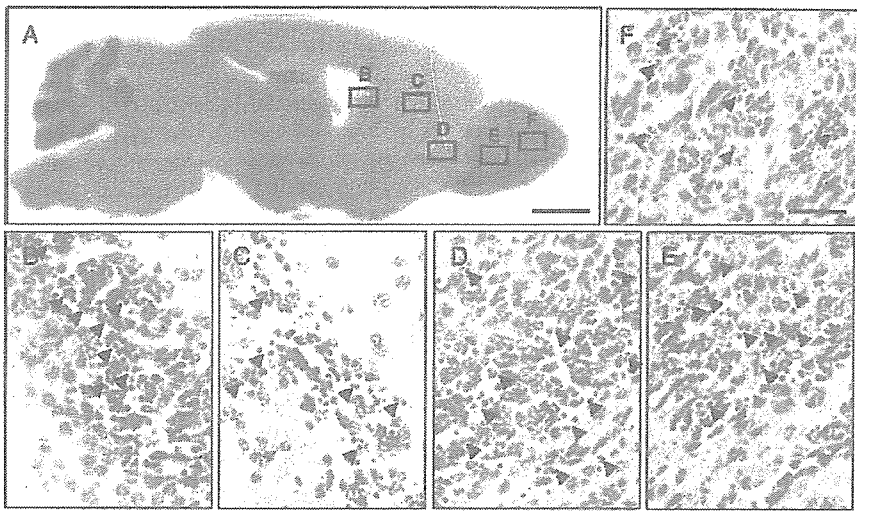

FIGURE 1. Apoptotic cell death in the subventricular zone (SVZ) and rostral migratory stream (RMS) and its extension to the olfactory bulb (OB). Hematoxylin and eosin (H&E) staining. **(A)** A representative sagittal brain section from an MPTP-treated mouse killed at 24 hours after MPTP injection. **(B–F)** Higher magnification of the boxed areas in **(A)** reveals that the majority of cells exhibit apoptotic characteristics (i.e. nuclear condensation and fragmentation) in the SVZ **(B)**, RMS **(C, D)**, and OB **(E, F)**. Scale bar = **(A)** 2 mm, **(B–F)** 50 μm.

Apoptosis Detection Kit and an ApopTag peroxidase In Situ Apoptosis Detection Kit (Chemicon) according to the manufacturer's instructions.

TUNEL Double-Labeling Immunofluorescence

Subsequent to visualization of the fragmented DNA using the fluorescent TUNEL method, sections were incubated in 10% normal goat serum and 0.40% Triton X-100 in phosphate-buffered saline (PBS) for 1 hour at room temperature. A rabbit monoclonal anti-Iba 1 antibody was then applied overnight. After being washed in PBS, sections were incubated with a biotinylated secondary goat anti-rabbit IgG antibody (1:100; Vector Laboratories) for 1 hour at room temperature followed by Texas red-avidin D

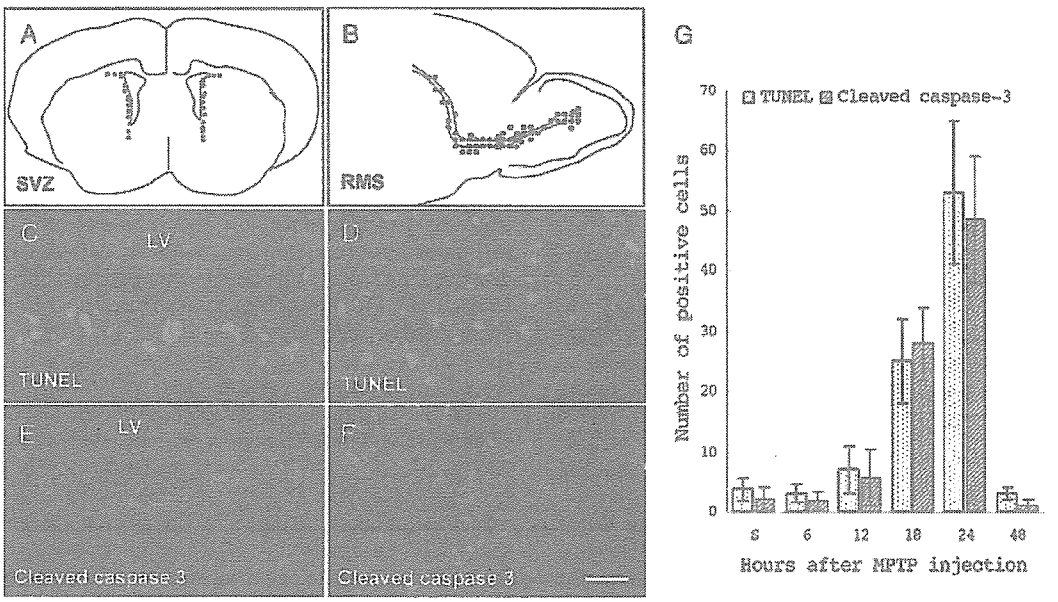

FIGURE 2. Detection of apoptotic cells in the subventricular zone (SVZ) (coronal section) and rostral migratory stream (RMS) (sagittal section) with fluorescence TUNEL and immunofluorescence staining for cleaved caspase-3. **(A, B)** Schematic distribution of apoptotic cells in the SVZ and RMS with the positions of the cells undergoing apoptosis indicated by dots. **(C, D)** Apoptotic nucleus (green) in the SVZ and RMS revealed by the TUNEL technique and **(E, F)** cleaved caspase-3 staining (red) in the same field. Scale bar = 50 μm. **(G)** The results of a quantitative analysis of TUNEL-positive or cleaved caspase-3-immunoreactive cells in the SVZ of MPTP-treated group. The number of TUNEL-positive or cleaved caspase-3-immunoreactive cells peaked at 24 hours and had declined to very low levels by 48 hours after MPTP injection. Neither TUNEL-positive nor cleaved caspase-3-immunoreactive cells were found in control animals at any time point. The number of positive cells in the unilateral SVZ was counted in 3 to 5 different brains. S, saline-treated control; LV, lateral ventricle.

for 1 hour at room temperature. Sections were then mounted with Vectashield and observed using the Zeiss LSM510 confocal laser scanning microscope.

Electron Microscopic Observation

The brain samples were immediately removed and fixed in 2.5% glutaraldehyde in 0.1 M phosphate buffer, postfixed in 1.0% osmium tetroxide/0.1 M phosphate buffer, and embedded in Epon 812. Ultrathin sections of the areas of interest were cut with a diamond knife, double-stained with uranyl acetate and lead citrate, and examined under the JEM-1200EX electron microscope (JEOL) at 60 kV.

Cell Counting and Statistics

Serial brain coronal sections through the SVZ corresponding to bregma from 0.50 to 0.98 mm (anterior–posterior coordinate) were collected with the aid of the mouse brain atlas (33). At least one of every 15 sections (total 5 to 7 sections per animal) was blindly counted for quantitative analysis on DAB-stained (cells positive for TUNEL, cleaved caspase-3, GFAP, Dcx, or Iba 1) sections. Results were expressed as the average number in the unilateral SVZ and reported as the mean ± standard deviation. The Student *t*-test was used to assess differences between data groups. Differences were considered statistically significant of $p < 0.05$.

RESULTS

Induction of Apoptosis After a Single Injection of MPTP

Histologic Findings

The criteria defined by nuclear condensation (pyknosis) and nuclear fragmentation (karyorrhexis) were used to identify apoptotic cell death in H&E-stained, paraffin-embedded sections. Numerous apoptotic bodies were observed in the forebrain of C57BL/6 mice 24 hours after the administration of MPTP (Fig. 1), but none in the saline-administered controls. The induction of apoptosis by MPTP was restricted to the SVZ (Fig. 1B), RMS (Fig. 1C, D), and OB (Fig. 1E, F). No such changes were found in any other regions of the brain.

TUNEL Assay

Figures 2A and 2B show the schematic distribution of MPTP-induced apoptosis in the SVZ and RMS with the positions of the cells undergoing apoptosis indicated by dots. Representative photographs of TUNEL-positive sections are shown in Figures 2C (SVZ) and 2D (RMS). Time course response experiments were also carried out. Figure 2G depicts the peak levels of apoptosis in the SVZ at 24 hours after the administration of MPTP. By 48 hours, the number

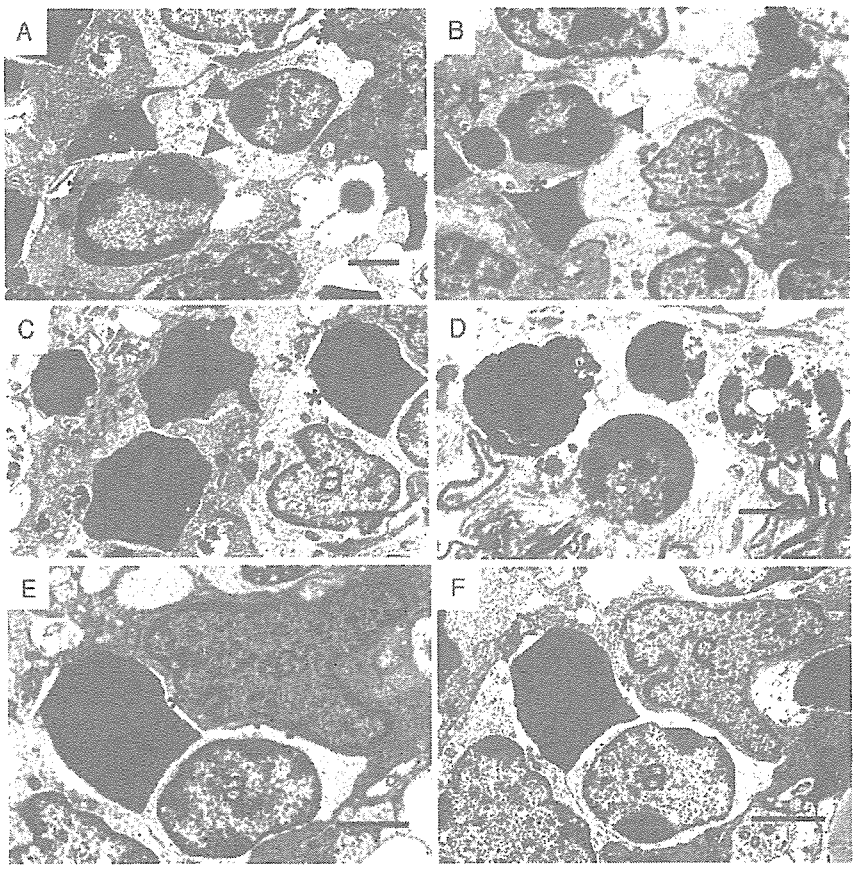

FIGURE 3. Electron micrographs of the subventricular zone **(A–C, E, F)** and rostral migratory stream **(D)** obtained from a MPTP-treated mouse. **(A, B)** Early and midstage of apoptotic changes included the dense aggregation of nuclear chromatin **([A, B]**, arrowhead) and formation of apoptotic bodies **([B]**, arrow). **(C– F)** Advanced-stage apoptotic cells exhibited marked chromatin condensation and cellular shrinkage with or without disruption of the plasma membrane. The cells undergoing apoptosis were identified morphologically as migrating neuroblasts according to the criteria defined by Doetsch et al (19), i.e. an open pericellular space **([A–C, E, F]**, asterisks), a scant and dark cytoplasm, and smooth contours. The adjacent typical migrating neuroblasts **(B–C, E, F, a)** are still alive. Type C cells, which have an irregular nucleus with deep invaginations, mostly lack chromatin and have a typical and large reticulated nucleolus **(A, B, E, F, c)** were also observed. Scale bar = 2 μm.

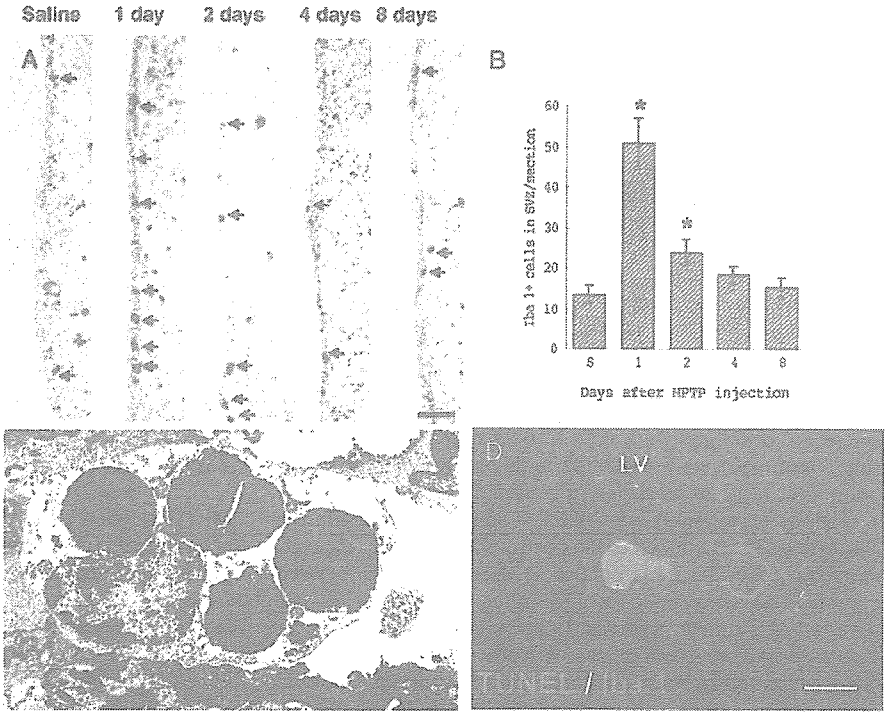

FIGURE 4. Evidence for phagocytosis of apoptotic cells by microglia cells in the subventricular zone (SVZ). Representative sections were immunostained for Iba 1 showing microglial infiltration to the SVZ (**[A]**, arrows). A significant increase in the number of Iba 1-immunoreactive cells by 1 and 2 days after MPTP injection compared with controls was recorded with a decline to the control level by 4 and 8 days **(B)**. **(C)** Representative electron microphotograph showing an activated microglial cell (arrowhead) with an enlarged cytoplasm, which contains several ingested apoptotic bodies. **(D)** Microphotograph of TUNEL double-labeling with the antibody for Iba 1 showing apoptotic bodies (TUNEL-positive, green) phagocytosed by a microglial cell (Iba 1-positive, red). Data are expressed as means ± standard error of mean. *, $p < 0.05$ compared with saline-treated control. The numbers of Iba 1^+ cells in the unilateral SVZ were counted in 3 to 5 different brains. Scale bars = **(A)** 50 μm; **(C)** 2 μm; **(D)**6 μm. S, saline-treated control; LV, lateral ventricle.

of apoptotic cells had declined remarkably. The same changes were observed in the RMS. Very few TUNEL-positive cells were detected in the SVZ and RMS in saline-treated mice.

Distribution of Cleaved Caspase-3

Immunohistochemical staining for cleaved caspase-3 demonstrated a marked increase in reactivity in the SVZ and RMS at 24 hours after MPTP was administered, paralleling

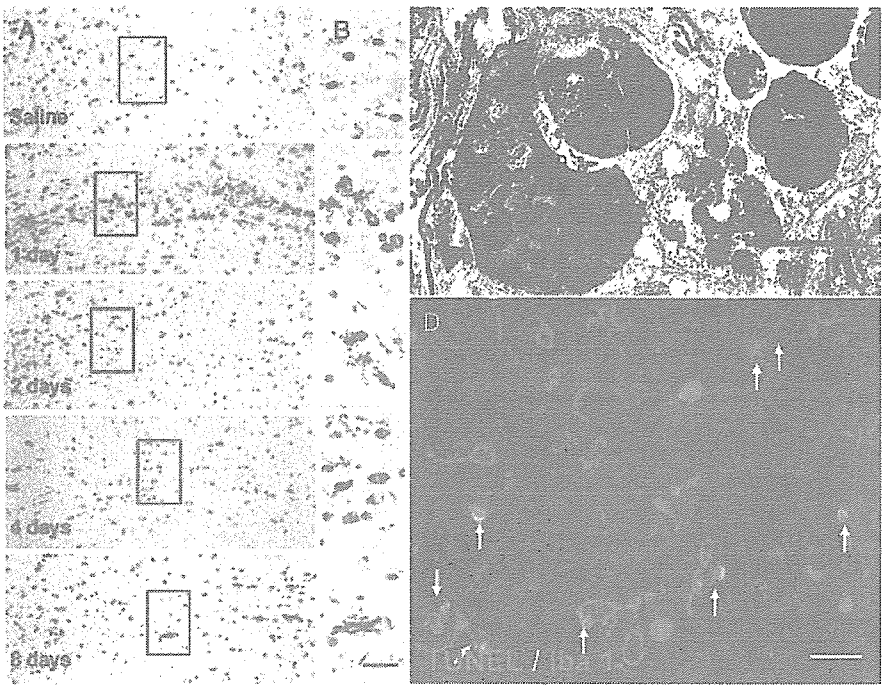

FIGURE 5. Evidence of phagocytosis of apoptotic cells by neighboring microglia in the rostral migratory stream (RMS). Representative sagittal sections through the RMS were immunostained for Iba 1 showing microglial activation and infiltration of the RMS at 1, 2, 4, and 8 days after MPTP administration **(A, B)**. **(B)** Higher magnification of boxed areas from **(A)**. **(C)** Representative electron microphotograph showing an activated microglial cell (arrowhead) with an enlarged cytoplasm phagocytosing an apoptotic body. **(D)** Microphotograph of double-labeling with TUNEL and the antibody for Iba 1. Many TUNEL-positive (green) apoptotic bodies were phagocytosed by microglial cells (Iba 1-positive, red). Scale bars = **(A, B)** 20 μm; **(C)** 2 μm; **(D)** 10 μm.

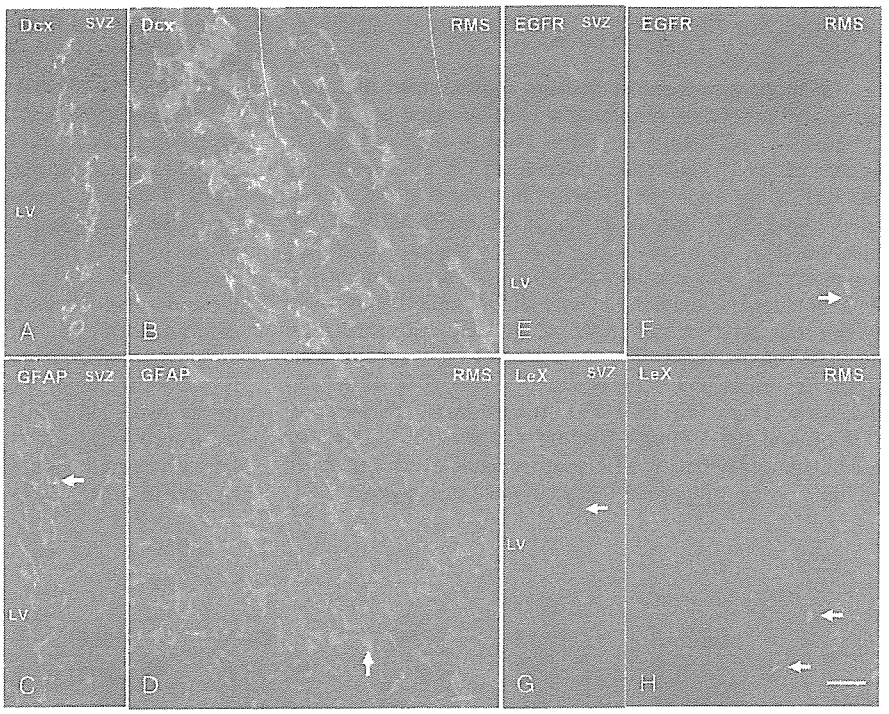

FIGURE 6. Phenotypic analysis of cells undergoing apoptosis in the subventricular zone (SVZ) and rostral migratory stream (RMS). Representative microphotographs of the SVZ coronal **(A, C, E, G)** and RMS sagittal sections **(B, D, F, H)** obtained from MPTP-treated mice and double-labeled for cleaved caspase-3 (red) and a migrating neuroblast marker Dcx **([A, B]**, green), an astrocyte marker GFAP **([C, D]**, green), and a transit-amplifying precursor marker EGFR **([E, F]**, green) or LeX **([G, H]**, green). The majority of cleaved caspase-3-positive cells in the SVZ **(A)** and RMS **(B)** expressed Dcx; however, a few cleaved caspase-3-positive cells expressed GFAP in the SVZ **([C]**, arrow) and RMS **([D]**, arrow). Cells expressing cleaved caspase-3 were not labeled for either EGFR **(E, F)** or LeX **(G, H)**. Scale bars = **(E)** 10 μm; **(A–D, F–H)** 20 μm. LV, lateral ventricle.

the change in the numbers of TUNEL-positive cells. Time course-dependent changes in the number of cleaved caspase-3-immunoreactive cells in the SVZ are shown in Figure 2G. Figures 2E and 2F show representative photographs of the expression of cleaved caspase-3 in coronal and sagittal sections obtained from an MPTP mouse. Very few cells expressing cleaved caspase-3 were detected in the SVZ or RMS in saline-treated mice.

Ultrastructural Demonstration of Apoptosis

Electron microscopy of brain tissues obtained from MPTP-treated mice revealed cells in the SVZ and RMS with ultrastructural characteristic of the early to midstages of apoptosis, including dense aggregates of chromatin and apoptotic bodies (Fig. 3A, B). Cells in advanced stages of apoptotic death exhibited marked chromatin condensation and cellular shrinkage with or without disruption of the plasma membrane (Fig. 3C–F).

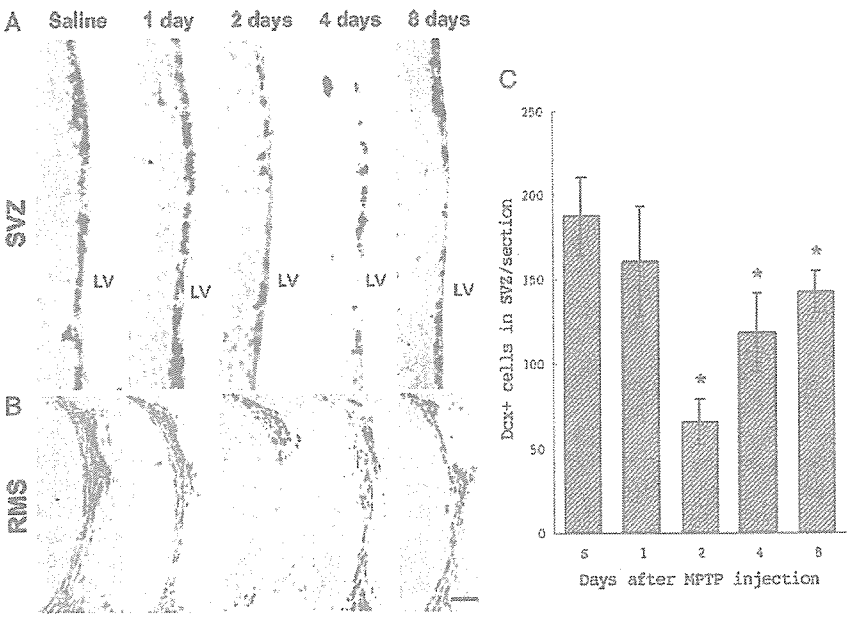

FIGURE 7. Reduction in numbers of migrating neuroblasts in the subventricular zone (SVZ) and rostral migratory stream (RMS). Representative microphotographs of coronal and sagittal sections immunostained for Dcx in the SVZ **(A)** and RMS **(B)** obtained from MPTP-treated mice killed at 1, 2, 4, and 8 days after MPTP injection. Scale bars = **(A)** 50 μm; **(B)** 100 μm. Controls received saline only. A marked decrease in Dcx-immunoreactive neuroblasts at 2, 4, and 8 days after MPTP administration compared with controls **(C)**. Data are expressed as means ± standard error of mean. *, $p < 0.05$ compared with saline. The numbers of Dcx^+ cells in the unilateral SVZ were counted in 3 to 5 different brains. S, saline control; LV, lateral ventricle.